X-616-68-166

LUNAR EXPLORER 35*

Norman F. Ness
Laboratory for Space Sciences
NASA-Goddard Space Flight Center
Greenbelt, Maryland USA

May 1968

*Presented at XIth COSPAR Tokyo, Japan; 16 May 1968

Extraterrestrial Physics Branch Preprint Series

LUNAR EXPLORER 35

Norman F. Ness
NASA-Goddard Space Flight Center
Greenbelt, Maryland USA

Abstract

Lunar Explorer 35, a 104 Kg spin stabilized spacecraft, was placed in lunar orbit on 22 July 1967 with period = 11.5 hours, inclination = 169°, aposelene = 9388 ± 100 km, periselene = 2568 ± 100 km, and initial aposelene-moon-sun angle = 304°E. The experiment repertoire includes magnetometers, plasma probes, energetic particle and cosmic dust detectors. Bi-static radar measurements of the electromagnetic properties of the lunar surface have been studied by monitoring the transmitted and reflected RF signal. The spacecraft has operated continuously since launch and has provided new and illuminating data. During its orbit about the earth, the moon is immersed in either interplanetary space or the geomagnetosheath-geomagnetotail formed by the solar wind interaction with the earth. In the geomagnetotail no evidence is found for a lunar magnetic field limiting the magnetic moment to 10^{20} cgs units (less than 10^{-6} of the earth). In the interplanetary medium no evidence is found for a bow shock wave due to supersonic solar wind flow. The moon does not accrete interplanetary magnetic field lines as theorized by Gold and Tozer, and as reported from Luna 10 measurements. A plasma shadow or cavity develops on the anti-solar side of the moon. Small magnetic field perturbations consisting of penumbral increases and decreases but only umbral increases are observed due to the diamagnetic properties of the plasma. Diffusion of interplanetary field lines through the lunar body indicates a low electrical conductivity for the outer layers of the moon, less than 10^{-5} mhos/m., and correspondingly low body temperatures. This paper reviews the scientific results from this satellite mission.

1.0 Introduction

During 1963-1965 the small spin stabilized satellites Explorers 18, 21 and 28 represented the initial phase of the USA IMP (Interplanetary Monitoring Platform) program to study the geophysical environment of the earth from highly eccentric orbit. These satellites provided definitive measurements of the interplanetary medium, the interaction of the solar wind with the geomagnetic field forming a collisionless detached MHD bow shock and the extension of the geomagnetic field into interplanetary space forming the geomagnetic tail.

The initial attempt to study the environment of the moon by anchoring an IMP type satellite in lunar orbit in 1966 failed with Explorer 33 placed instead into an extremely high apogee-perigee earth orbit from which significant scientific results have been obtained. The second attempt on 19 July 1967 was successful with Explorer 35 placed into lunar orbit on July 22 with orbital period 11.53 hours, inclination 169° with respect to the ecliptic plane, aposelene = 9388 $\pm$ 100 km (5.4 R_M, R_M = Radius of Moon = 1738 km) periselene = 2568 $\pm$ 100 km (1.4 R_M) and initial aposelene-moon-sun angle = 304° East.

Figure 1 presents the projection of the orbit on a plane passing through the center of the moon and parallel to the ecliptic plane, which defines a selenocentric solar ecliptic coordinate system with the X_{SSE} axis directed from the moon to the sun and the Z_{SSE} axis perpendicular to the ecliptic plane. The variation of the orbit geometry is due to the heliocentric motion of the earth-moon system and leads to an apparent westward progression of the line of apsides of approximately 1.1° per day.

Explorer 35 is spin stabilized at 25.6 $\pm$ 0.4 RPM with the spin axis perpendicular to the ecliptic plane $\pm$ 2^{o}. The spacecraft is powered primarily by solar cells on four paddles which provide 70-80 watts of power, sufficient to permit continuous transmission of scientific data. During passage through the optical shadow of the moon, lasting for intervals up to 60 minutes, battery power is sufficient to continuously transmit scientific data. The experiment repertoire includes two fluxgate magnetometers, two plasma probes, two energetic particle detectors and one cosmic dust detector. Two passive experiments utilize the spacecraft for a study of the gravitational field of the moon by analysis of its orbital characteristics and bistatic radar measurements of the electromagnetic properties of the lunar surface by monitoring the directly transmitted and lunar surface reflected RF signal at 136 mHZ. A detailed discussion of the technical aspects of the spacecraft and the telemetry system, data readout and the experiments is given in (14).

The spacecraft has operated continuously since launch and successfully survived the complex and extended shadow periods during the lunar eclipses of 18 October 1967 and 13 April 1968. The spacecraft has completed more than 600 orbits of the moon and as noted in fig. 1 has provided direct measurements insitu of the lunar environment over a large region. A discussion of the detailed performance of the spacecraft is available in (13). It is the purpose of this paper to briefly summarize and present representative data concerning the scientific results and conclusions obtained thus far.

2.1 NASA-GSFC Low Energy Plasma Measurements

Measurements of the magnitude and polarity of the plasma currents for energies between $\pm$ 50 volts were performed by means of a planer geometry multiple grid retarding potential analyser (22). Representative results obtained both in sunlight and shadow are shown in fig. 2. A two component Maxwellian distribution of the electron spectrum is observed with the energetic component corresponding to solar wind electrons at a temperature of $7.1 \times 10^4\,^{o}K$ and density $6/cm^3$.

A low energy component is also observed with a temperature of $10^4\,^{o}K$ and is interpreted as a photo-electron cloud enveloping the spacecraft due to solar ultraviolet illumination. The low energy component observed in lunar shadow may possibly be due to high energy electron bombardment. The ion mode current is virtually zero in lunar optical shadow, equal to the instrument noise level.

From these data, a measurement of spacecraft to plasma potential is obtained which indicates a change from -2 volts in sunlight to -4 volts in shadow. This is consistent with the expectation that solar UV causes a rise in satellite potential due to photo-electron emission from the surface of the spacecraft.

A series of electron mode spectra obtained as the spacecraft passes through lunar shadow is shown in fig. 3. The numbers along the orbital path refer to the sequential time order in which the spectra were obtained. A measure of the solar wind electron temperature of $8.4 \times 10^4\,^{o}K$ is obtained for spectra 1 (one) and 2 which indicates no

appreciable cooling of the electron component of the plasma as it expands into the lunar shadow. The relative density of the electrons with respect to their value in the interplanetary medium decreases from 7% at 1 (one) to 3% at 2 and a minimum of less than 1% at locations 3 and 4. This density decrease towards a minimum almost coincident with the geometric core of the umbra is characteristic of the lunar shadow. No evidence is found in this experiment for the existence of a lunar bow shock which would give rise to a thermalized sheath of plasma or particle fluxes associated with the moon.

2.2 MIT-High Energy Plasma Measurements

The MIT plasma experiment employs a Faraday cup type detector with a split collector to measure the flux of both positively and negatively charged particles in the energy (E) to charge (Q) ratio of $50 \leq E/Q \leq 5400$ volts (11,12). The detector is mounted with the cup axis perpendicular to the spacecraft spin axis and the response in the meridian plane falls to 0 at $\pm 60^{\circ}$. A 1 (one) KHZ modulated wave form applied to the multigrid detector provides energy discrimination. A series of 7 differential energy spectra measurements are made as well as an integral mode which measures the total flux at 27 sequential data points each separated by 0.16 seconds. The satellite rotates approximately 27° between successive points and this provides 360° directional information of the bulk flow at 164 second intervals.

A series of integral data samples in the ion mode obtained on 27 July 1967 is shown in fig. 4. At this time, the moon was imbedded

within the undisturbed solar wind and the roll modulation of the measured current is clearly evident indicating a directed flow of solar plasma. Because of the asynchronism between the spin rate and telemetry readout, the peak current appears at a progressively different time within successive readouts. The peak current measured is essentially constant until sequence 22867 when a decrease to a minimum value at the instrumental noise level is reached at sequence 22875. The current remains below noise level until sequence 22897 when the current recovers to that prior to the shadow passage. These data do not show any evidence of a change in character which can be interpreted as a passage through a bow shock encompassing the moon.

Projection of the corresponding orbital data is given in fig. 5 with the decimal times corresponding to the locations on the orbit indicated by dots. The perturbed periods of plasma flow taken from fig. 4 are indicated and compared to theoretical models of nonmagnetized cold solar wind flow assuming a bulk velocity of 350 km/sec and to a moderately hot solar wind flow with a thermal speed of 50 km/sec. The initial conclusions drawn from these data are that the moon carves out a cavity in the solar wind by absorbing the impacting plasma and that this plasma cavity closes behind the moon in a manner consistent with the expected particle thermal speeds. Occasionally there appear to be temporary "puffs" of plasma observed when the spacecraft is well within the lunar plasma wake. It is expected that these anomalous conditions are intimately related to the interplanetary magnetic field topology and its temporal behavior.

Data obtained from passage through the lunar wake region on November 27-28, 1967 are shown in fig. 6. Here the split collector "A+B" and "A-B" current samples are plotted as in fig. 4 but with compressed horizontal time scales. After a careful study it has been determined that there is no significant change in the plasma flow characteristics from solar wind conditions. This appears to indicate that the lunar wake is essentially not observable more than 5-10 R_M downstream from the lunar body.

2.3 NASA-GSFC Triaxial Fluxgate Magnetometer

A sensitive triaxial fluxgate magnetometer with automatic range switching provides detailed measurements of the vector magnetic field at intervals of 5.12 seconds and a sensitivity of $\pm$ 0.1γ (19, 20,21). Reduction of directional references on the spacecraft during lunar shadow are complicated due to the loss of timing reference signals with respect to a spacecraft sun direction. In spite of a pseudo-sun pulse system providing an approximate timing reference, the analysis is further complicated by a variable spin rate of the spacecraft in shadow due to thermal contraction and conservation of angular momentum. A detailed study of this phenomenon and a numerical analytical technique for rectification of directional measurements in the optical shadow of the moon has been conducted (24).

Vector measurements are presented in fig. 7 for two orbital passes through the lunar shadow on 31 July and 4 August 1967. These data illustrate the different types of magnetic field anomalies

detected in lunar orbit while the moon is located in the interplanetary medium. In the upper half essentially no perturbation of the interplanetary magnetic field is observed indicating that the moon does not permanently accrete the interplanetary magnetic field as theorized (7,25) and reported experimentally from Luna 10 (6).

The data presented in the lower portion of fig. 4 show that as the spacecraft passes through the disturbed plasma wake region perturbations of the interplanetary magnetic field magnitude are observed. Characteristically increases in the magnitude are observed in the lunar umbral core while in the penumbral region decreases and some times, as here, exterior increases are also observed. No evidence is found for the occurrence of a lunar bow shock wave in some 150 interplanetary orbital passes which have been analyzed thus far (19,20). The interplanetary magnetic field appears to be convectively transported past the moon by the solar plasma with small perturbations due to the lunar wake evident in varying degrees depending upon interplanetary conditions (21).

Data obtained on the orbital pass of 4 December 1967 when Explorer 35 passed through the downstream wake at $\sim 5\ R_M$ are presented in fig. 8. Observations from the NASA-GSFC experiment on Explorer 33 are superimposed with a time offset determined by the directional discontinuities simultaneously detected near 0400. A small but clearly evident decrease in the magnitude of the field is evident in the lunar wake with a broad minimum near 0530. Since the spacecraft does not pass

through the umbral core of the lunar wake no increase is detected. These data also show that there appears to be no detectable shock wave trailing the moon as recently theorized (15,16). These results do not support the tentative IMP-1 observations (17) of a lunar associated wake at 150 R_M.

When the moon is imbedded in the geomagnetic tail it is optimumly possible to detect any intrinsic magnetic properties of the lunar body. Data obtained from a detailed study (3) are shown in fig. 9 for a "quiet" time as the spacecraft passes through periselene. The theoretical curve shown corresponds to superposition of a geomagnetic tail field of 9γ and a lunar magnetic moment of 10^{20} cgs units. Inspection indicates the observed perturbations are less than would be predicted with the parameters. This result is a factor of 60 lower than established by the Luna 2 results and the preliminary Explorer 35 results (4,19). This indicates that the intrinsic magnetic field of the moon is less than 4γ on the surface and that in general the lunar magnetic field environment on the surface is dominated either by the geomagnetic tail, magnetosheath or interplanetary magnetic field depending upon the position of the moon relative to the geomagnetosphere. In addition, these data can be analyzed for magnetic susceptibility and the result obtained is that μ_M is less than $1.8\mu_o$ if the lunar body is homogeneous (3).

2.4 NASA-ARC Triaxial Fluxgate Magnetometer

Measurements of the near lunar magnetic field were made by a second triaxial fluxgate magnetometer with three ranges that was sequentially programmed once every 6.1 seconds with maximum sensitivity of [illegible] $\pm$ 0.2 γ (4,5). Results from this experiment indicate the absence of an appreciable lunar field due to the moon at satellite altitudes of a few gammas, limiting the magnetic moment to 6 x 10^{20} cgs units (4).

Representative data in August 1967 are presented in fig. 10 as the spacecraft passes through the lunar wake in the interplanetary medium. Noted here, relative to the time of entry into the optical shadow, are the increased magnitude of the field in the umbral region and the decreases in the penumbral region. The data are normalized to a mean interplanetary field magnitude of 6.6γ for orbits 28, 32, 35, and 38. The criteria for superposition emphasized the relative position of the dips at the edges of the shadows and the corresponding spread of optical shadow times is shown by vertical bars. No evidence for a bow shock is obtained from these data (4,5).

A summary of features observed during the lunar orbits when the moon is outside the earth's bow shock is shown in fig. 11. The abscissa represents the orbit number with the ordinate representing the time of observation relative to the time of entrance of the spacecraft into optical shadow. The higher numbered orbits pass through the shadow at greater lunar distances and also farther north from the moon-sun line. Plateau edges are identified in cases where

the field magnitude peak is broad and relatively flat and where the plateau edges are relatively isolated from other features. The dips represent those positions where the field magnitude minima are observed near the boundary of the lunar shadow. Peaks of the magnitude external to the dips are also identified either by the location of the maxima or in some cases by the location of the sharp outer boundary (5).

2.5 U. of California, Berkeley-Energetic Particle Measurements

Detailed measurements of energetic electrons, protons and X-rays have been performed by two experiments on Explorer 35. The University of California, Berkeley experiment consists of a 4" Neher type integrating ion chamber and two thin windowed Geiger-Mueller tubes (10). One GM tube observes the particle flux scattered off a gold foil and hence its response is limited to electrons Ee > 45 kev. A second GM tube contains a 0.7 mg/cm^2 mica window and responds to protons Ep $\geq$ 300 kev and electrons Ee $\geq$ 22 kev. The ion chamber is sensitive primarily to protons Ep > 15 Mev. Both GM tube view axes are approximately parallel to the spacecraft spin axis with 70^o full-width-half-maximum directional response characteristics. Energetic particle counts are accumulated over many spin periods of the spacecraft.

No lunar associated energetic particle fluxes which might be expected in the case of an intrinsic or an accreted lunar magnetic field have been identified. However, energetic particle fluxes associated with the earth's bow shock, magnetosheath and magnetic tail are observed when the moon traverses these regions (2).

The moon is observed to act as a passive shield and absorber of charged particles and decreases in these fluxes are observed by Explorer 35 at favorable locations in the satellite orbit. The shielding effect of the moon for energetic particles depends on the size of their gyroradii, hence their energy and pitch angle distribution. For isotropic fluxes, such as galactic cosmic rays, the decrease in flux observed is simply the percentage of the solid angle subtended by the moon at the satellite orbit. Fig. 12 presents the calculated variation of the galactic cosmic ray background as the spacecraft passes through periselene as well as the observed ion chamber count rate for several orbits. The theoretical calculation omits any contribution of cosmic ray lunar albedo and predicts a decrease of 13% since the moon subtends approximately 1.69 steradians at periselene.

Solar flare electron fluxes have been shown to be highly anisotropic and thus when the moon is on the same magnetic field line as the satellite, it can completely absorb all of the electrons which propagate from a direction opposite to the satellite. The geometry of field lines threading the moon is shown in fig. 13.

A representative sample of occultation of solar electron flux by the moon is shown in fig. 14. Here particle and magnetic field data are compared. The scatter counter shows a decrease in count rate to a level corresponding to penetrating cosmic ray background indicating essentially no electrons observed during the occultation when $D < 1650$ km and $\Delta < -10^{\circ}$. This shows that the field lines are threading the moon and that in the lunar wake they have at most a

small curvature since the assumption of rectilinear field lines is made to compute D and Δ.

Similar observations have been conducted in the geomagnetic tail regions following solar flares. When the spacecraft is in front of the moon with respect to the sun and earth, decreases are observed which have been interpreted (10) to indicate that the electrons gain access to the geomagnetic tail at a point beyond the lunar orbit. These solar flare electrons normally propagate up the tail towards the magnetosphere and presumably are lost close to the earth.

2.6 U. of Iowa-Energetic Particle Measurements

The University of Iowa energetic particle experiment utilizes GM tubes and solid state detectors to measure the flux of electrons Ee > 45 kev and protons Ep $\geq$ 322 kev (27). Directional measurements in the ecliptic plane are obtained through the use of 4 separate counters, each having an azimuthal acceptance angle of 90^{o}. A thorough analysis of more than 350 orbits about the moon has established the absence of detectable intensities ($j \geq 5/cm^2$ sec sterad) associated with the moon. The conclusion is reached that there are no strong shock effects associated with the interaction of the solar wind with the moon that generate energetic particle spikes such as associated with the earth's bow shock front and within the magnetopause of the earth.

Shadowing effects of the moon on protons are consistent with purely geometric considerations consistent with their large gyroradii (R_L) in the ambient interplanetary or geomagnetic tail field ($R_L > 10\ R_M$). However, shadowing effects on electrons are much more complex due to their small gyroradii ($< 0.1\ R_M$). Such effects have provided a method of magnetic field line tracing from the spacecraft to the moon and preliminary results (27) indicate that

(a) Magnetic field lines pass through the moon or at least directly to its surface with an angular deviation of less than 0.1 radian in a distance of 1.5 R_M and,

(b) Electrons appear to diffuse transverse to the magnetospheric tail with $v_\perp \leq 100$ km/sec in the region between the earth and the moon. This implies an upper limit on the transverse component of the electric field less than 10^{-3} volts/meter.

Shortly after the onset of a solar electron event, the angular distributions are usually markedly anisotropic with a maximum intensity well collimated along a local magnetic field vector and flowing outward from the sun. This angular distribution generally relaxes toward an isotropic one within 1 to 2 hours. An especially valuable sequence of such events were observed during late July and early August from McMath plage region 8905 and are summarized in Table I. Many of these events have been observed simultaneously with Explorer 33 and the heliocentric spacecraft Mariner 5.

A study of the time history, intensity and angular distribution of solar emitted protons and alpha particles has been conducted for the period 19 July to 31 December 1967. A noteworthy finding is that during this period interplanetary space is seldom free of a measurable intensity ($j \geq 0.1/cm^2$ sec sterad) of protons ($Ep \geq 322$ kev). Clear examples of corotating beams of solar protons extending over large heliocentric longitudes are found in addition to many cases of a different nature suggesting simultaneous emission of particles over large angular spreads exceeding 60^o as measured by heliocentric longitude.

A continuous recording of the absolute intensity of solar X-rays from the disk of the sun is obtained except during optical eclipses of Explorer 35 by the moon. A joint study of the solar X-ray and radio emissions is being conducted with emphasis on conditions in the solar atmosphere. A detailed profile of the X-ray eclipses observed on 18 October 1967 and 13 April 1968 is being used to determine the distribution of X-ray emissivity on the solar disk.

The absolute intensity and angular distribution of alpha particles $2.0 \leq E_\alpha \leq 10.2$ mev has been obtained by a solid state detector making it possible to estimate the emissivity of alpha particles from the radioactive gases thoron and radon of the tenuous lunar atmosphere. A provisional upper limit from the analysis of two months of data is that $\sigma \leq 10^{-2}/cm^2$ sec sterad.

2.7 Stanford-Lunar Ionosphere and Radio Wave Propagation Experiment

Monitoring of the telemetry transmittor of Explorer 35 at 136 mHZ has been conducted by Stanford University using the transmitter as a radar beacon to remotely probe the electromagnetic properties of the moon's surface (26). Radio signals which originate on the spacecraft are reflected from the lunar surface and both directly transmitted and lunar surface reflected signals are received at the Stanford antenna facilities. The experimental geometry is illustrated in fig. 15 for several positions of the satellite relative to the moon-earth line. The angle ϕ corresponds to the angle of incidence at the lunar surface and it is seen that it varies depending upon the position of the spacecraft in selenocentric orbit.

As the spacecraft revolves around the moon the reflection point moves across the lunar surface at varying angles of incidence. Because the moon appears to be relatively smooth at the wave lengths employed, the reflection characteristics are principally dependent upon a small area only a few kilometers in extent. As the spacecraft passes behind and is occulted by the moon, a diffraction pattern is observed in the received signal. A comparison of the theoretical pattern due to a knife edge with that observed by Explorer 35 is shown in fig. 16. These occultation immersion and emersion observations are important with respect to the determination of the tenuous properties of a lunar ionosphere. No positive results as yet have been obtained although the discrepancies observed in fig. 16 clearly indicate that a knife edge approximation is not sufficient.

The variation of the reflectivity versus angle of incidence is shown for both right and left hand circular polarizations in the upper portion of fig. 17. The data were obtained on two days exactly one lunation apart with the variation in the response correlating with movement of the reflection point from highlands to the maria and back. A greater reflectivity is found in the maria and the general trend upward in reflectivity corresponds to motion of the reflection point onto relatively younger maria material in the region of Flamsteed. It is concluded that on the whole, the moon is a remarkedly homogeneous body with respect to reflection of electromagnetic signals at 136 mHZ. Typical variations are on the order of 30% although larger changes are occasionally observed. These variations are one order of magnitude less than what would be observed on the surface of the earth.

In the lower half of fig. 17 are presented results pertinent to measurement of the Brewster angle of the lunar surface. This curve is the sum of the two circularly polarized scattered waves. The Brewster angle corresponds to that angle at which there is total absorption of linearly polarized waves and is found to be approximately 60^{o}. This implies a dielectric constant ϵ for the lunar surface of 3.0 ϵ_{o}.

2.8 Baylor and Temple U.-Interplanetary Dust

Measurements concerning the flux and velocities of aggregates of minute particulate matter in selenocentric space have been obtained from a large area acoustical transducer plate with a sensitivity of

approximately 5 pg at a velocity of 10 km/sec (1). A capacitor deposited on the impact side of the plate provides a signal from the device when the capacitor is completely penetrated. Data from these two sensors are presented in Tables II and III. In Table II a comparison is made from Explorer 35 results with those obtained from Lunar Orbiter and Mariner 4 which used a similar acoustical transducer in interplanetary space. These results appear to be consistent when consideration is given to the difference in mass threshold sensitivities. A second telescope detector measures the velocities of particles in a small time of flight analysis system. Particle velocities as low as 1.5 km/sec have been measured and interpreted to represent lunar ejecta.

The histogram shown in fig. 18 depicts the variation of impact events between 28 July 1967 and 28 February 1968. Three-fourths of the peaks in this histogram occur during the periods of known major meteor showers. Preliminary indications are that the instrument is measuring shower related lunar ejecta rather than an enhancement of the background event rates due to minute particles in the shower stream itself.

3.0 Theoretical Considerations and Results

Early models of the solar wind interaction with the moon (7,25) suggested accretion of the interplanetary magnetic field. These results have not been observed by Explorer 35 and no evidence for the existence of a pseudo-magnetosphere has been found. These results do not confirm

the report by Luna 10 of the existence of a pseudo-magnetosphere (6). The magnitude of the magnetic field in the vicinity of the moon lies generally between 5 to 8 γ when the spacecraft is in the undisturbed interplanetary medium and approximately 8 to 12 γ when the spacecraft is resident within the geomagnetic tail.

The magnetic field measurements combine with the plasma measurements to indicate that the solar wind directly impacts the lunar surface. It appears that the interplanetary magnetic field diffuses as rapidly through the lunar body as it is convectively transported past the moon by the solar wind. On the basis of these considerations a kinetic model of solar wind flow past the moon has been developed (28,29). The solar wind is approximated as a collisionless magnetized gas and the flow pattern past the moon is treated in the guiding center limit.

In this treatment the lunar wake behind the moon is not cylindrically symmetrical but a plane of symmetry is defined by the direction of the interplanetary magnetic field and the solar wind velocity. The height of the lunar wake remains constant at two lunar radii transverse to this plane while in this plane the width varies depending upon field orientation and the temperature of the plasma. An important parameter in this study is the speed ratio, S, defined by the ratio of the solar wind velocity, V_o, to the ion thermal speed parallel to the field lines, $v_{\|} = \sqrt{2kt_{\|}/m_i}$; $S = V_o/V_{\|}$.

The length of the wake varies depending upon the field orientation, $\emptyset$, with the shortest wake obtained when the field lines are transverse

to the solar wind flow. An infinitely long wake is predicted for a field line orientation parallel to the solar wind velocity with intermediate lengths obtained for oblique orientations.

An iterative approach to the solution of the MHD problem has been developed which begins with an ion wake computed on the assumption of zero perturbation of the interplanetary field (28). The ion wake obtained is utilized in a self-consistent solution of Maxwell's equations to determine the perturbation of the interplanetary magnetic field (21,29). Secondary electrical currents are induced in the disturbed plasma flow due to diamagnetic, field gradient and curvature currents. The most critical parameter determining the magnitude of the field anomaly at a given speed ratio and orientation is β, which is a measure of the diamagnetic properties of the plasma given by the ratio of perpendicular plasma pressure, $P_\perp = nmv_\perp^2/2$, to magnetic field pressure, $B^2/8\pi$: $\beta = 4\pi nm_i v_\perp^2/B^2$.

Representative results of the kinetic theory are shown in fig. 19 for a typical field orientation at the Archimedian spiral angle $\phi = 135^\circ$ and S = 10 for 3 values of β. Large values of β lead to enhanced perturbations of the field magnitude and are consistent with observations. The results do not predict the large amplitude oscillations in the penumbral region. It is expected that higher order iterations will be required to explain the perturbations observed exterior to the penumbral decreases. Computations of the β value of the interplanetary plasma obtained simultaneously by Explorer 34 (21) at the time of observations presented in fig. 7 yield

$\beta < 0.05$ and $\beta = 1.9$ respectively. A study of many orbital passes through the lunar wake simultaneous with observations by other satellites outside the lunar wake yield results depending upon field orientatation ϕ and plasma diamagnetism, β, similar to that predicted by the kinetic model.

Alternative approaches to the solar wind flow past the moon attempt to utilize an analogy with fluid dynamics (9,12,15,16). This approach predicts the existence of a trailing shock wave which has not been observed by either the MIT plasma probe or the NASA-GSFC magnetometer (see figs. 6 and 9). In addition, these studies cannot predict the observed exterior penumbral increases of field magnitude.

A modification of the fluid dynamic model has been suggested (12) which requires partial reflection of solar plasma at the surface of the moon. It is assumed that this reflection occurs along a narrow band near the solar plasma terminator on the lunar surface. While the physical nature of such a hypothetical interaction is subject to considerable debate, it appears that either small angle scattering from a neutral atmosphere or from a moderately enhanced local magnetic field could account for this effect. The net result is to predict enhanced field magnitudes and plasma densities in the penumbral regions which have been observed (12).

From simultaneous observations of the propagation of the interplanetary discontinuities past the moon it has been concluded (18) that the moon's average electrical conductivity is less than

10^{-5} mhos/m. if the moon is homogeneous and less than 10^{-4} mhos/m. if the moon consists of an insulating layer with a conducting core of radius 800 km. Complex effects of such a structure have been suggested (9) and a final conductivity structure not yet derived.

A study of the steady state configuration suggests that the electrical currents generated have the form of a simple linear unipolar generator (23). From a consideration of the maximum power available from the solar wind and for a homogeneous moon, the limit of saturation for typical solar wind parameters occurs when the electrical conductivity is in the range of 10^{-6} to 10^{-3} mhos/m.

4.0 Summary

The experimental results from Explorer 35 have definitively established the nature of the lunar environment and the solar wind flow past the moon. The moon appears to be a nonmagnetic, relatively nonconducting and hence relatively cold dielectric sphere which absorbs both solar wind plasma and energetic particle fluxes which impact its surface. A simplied diagram of the flow and field lines in the vicinity of the moon is given in fig. 20.

The electrical conductivity structure and internal temperature of the moon may be very interesting additional results obtained from Explorer 35. As additional studies are conducted of the experimental data and an accurate theoretical model developed for the propagation past the moon of transient disturbances, such as MHD shocks and tangential discontinuities, more precise insight into the problem of the present state of the lunar interior will be gained.

5.0 Acknowledgements

In preparing this brief summary of scientific results I have been assisted by the individual experimenters who, in many instances, provided advance copies of their preliminary reports for inclusion. I appreciate the cooperation of W. M. Alexander, K. W. Behannon, G. P. Serbu and Drs. E. F. Lyon, C. P. Sonett, H. E. Taylor, L. E. Tyler, and J. A. Van Allen.

6.0 References

1. Alexander, W. M. and J. L. Bohn, Initial Measurements from the Cosmic Dust Experiment, Trans. AGU 49, 243 (1968).
2. Anderson, K. A., Energetic Electrons of Terrestrial Origin at 60 R_E, Trans. AGU 49, 235 (1968).
3. Behannon, K. W., Intrinsic Magnetic Properties of the Lunar Body, Trans. AGU 49, 242 (1968).
4. Colburn, D. S., R. G. Currie, J. D. Mihalov and C. P. Sonett, Diamagnetic Solar Wind Cavity Discovered Behind Moon, Science 158, 1040 (1967).
5. Colburn, D. S., J. D. Mihalov, C. P. Sonett and S. H. Ward, The Lunar Cavity in the Solar Wind, Trans. AGU 49, 234 (1968).
6. Dolginov, Sh. Sh., Ye. G. Yeroshenko, L. N. Zhuzgov, and I. A. Zhulin, Possible Interpretation of the Results of Measurements in the Near Lunar Satellite AMS Luna 10, Geomagnetizm i Aeronomiya, 7, 436 (1967). (In Russian).
7. Gold, T., The Magnetosphere of the Moon, in The Solar Wind, edited by R. J. Mackin, Jr., and N. Neugebauer, 381, Pergamon Press, New York (1966).
8. Hundhausen, A. J., S. J. Bame and N. F. Ness, Solar Wind Thermal Anisotropies: Vela 3 and IMP 3, J. Geophys. Res., 72, 5265 (1967).
9. Johnson, F. and J. E. Midgley, Note on the Lunar Magnetosphere, J. Geophys. Res., 73, 1523 (1967).
10. Lin, R. P., Observations of Lunar Shadowing of Energetic Particles, J. Geophys. Res., 73, 3066 (1968).

11. Lyon, E. F., H. S. Bridge, J. H. Binsack, Explorer 35 Plasma Measurements in the Vicinity of the Moon, J. Geophys. Res., 72, 6113 (1967).

12. Lyon, E. F., G. S. Siscoe and H. S. Bridge, Explorer 35 Observations of the Solar Wind-Moon Interaction, MIT Center for Space Research Report CSR-TR-68-7 (1968).

13. Madden, J. J. and J. J. Brahm, Explorer 35 First Interim Report and Explorer 33 Third Interim Report and the AIMP Project Bibliography, NASA-GSFC preprint X-724-68-45 (1968).

14. Marcotte, P. G., J. J. Madden and J. J. Brahm, Anchored Interplanetary Monitoring Platform Summary Description for Explorer 33 AIMP-D and Explorer 35 AIMP-E, NASA-GSFC preprint X-724-68-82 (1968).

15. Michel, F. C., Shock Wave Trailing the Moon, J. Geophys. Res., 72, 5508 (1967a).

16. Michel, F. C., Magnetic Field Structure Behind the Moon, J. Geophys. Res., 73, 1533 (1967b).

17. Ness, N. F., The Magnetohydro dynamic Wake of the Moon, J. Geophys. Res., 70, 517 (1965).

18. Ness, Norman F., The Electrical Conductivity of the Moon, Trans. AGU 49, 242 (1968).

19. Ness, N. F., K. W. Behannon, C. S. Scearce, S. C. Cantarano, Early Results from the Magnetic Field Experiment on Lunar Explorer 35, J. Geophys. Res., 72, 5769 (1967).

20. Ness, N.F., K. W. Behannon, H. E. Taylor, Y. C. Whang, Perturbations of the Interplanetary Magnetic Field by the Lunar Wake, NASA-GSFC preprint X-612-68-12, (1968).

21. Ness, N. F. and K. W. Ogilvie, The Lunar Wake as a Solar Wind Sock, Trans. AGU 49, 242 (1968).

22. Serbu, P., Explorer 35 Measurements of Low Energy Plasma in Lunar Orbit, NASA-GSFC preprint (1968).

23. Sonett, C. P. and D. S. Colburn, Establishment of a Lunar Unipolar Generator and Associated Shock and Wake by the Solar Wind, Nature 216, 5113, 340 (1967).

24. Taylor, H. E., Aspect Determination in Lunar Shadow on Explorer 35, NASA-GSFC preprint X-612-67-611 (1967).

25. Tozer, D. C. and J. Wilson, The Electrical Conductivity of the Moon's Interior, Proc. Roy. Soc., A, 296, 320 (1967).

26. Tyler, G. L and A.M. Petterson, Bistatic Radar Measurements of the Dielectric Constant and EM Scattering Properties of the Lunar Surface, preprint (1968).

27. Van Allen, J. A. and N. F. Ness, Particle Shadowing by the Moon, University of Iowa preprint (1968).

28. Whang, Y. C., Interaction of the Magnetized Solar Wind with the Moon, NASA-GSFC preprint X-612-67-580 (1967).

29. Whang, Y. C., Theoretical Study of the Magnetic Field in the Lunar Wake, NASA-GSFC preprint X612-68-17 (1968).

Solar Electron Events

$j\ (E_e > 45\ keV) > 5\ (cm^2\ sec\ sr)^{-1}$

Mariner V, Explorer 33, Explorer 35

14 June to 30 November 1967

Date 1967	X-Ray Flare Onset	X-Ray Flare Max	Electrons Onset	Electrons Max	Δt min	j max $(cm^2\ sec\ sr)^{-1}$	Spacecraft 33	Spacecraft 35	Spacecraft V	Flare Region	Flare Lat	Flare Long	Flare Imp
28 July	01:00	01:28	02:01	02:14	61	120			X	8905	N25	E06	-N
	00:59	01:29	-	-	-	< 7		X					
	01:03	01:28	-	-	-	< 5	X						
29 July	08:18	08:30	08:47	09:10	29	120			X	8911	N25	E17	-N or
	-	-	> 08:30	08:47	> 12	290		X		8905	N24	W15	IN
	-	-	08:32	08:51	14	220	X						
	Other smaller and less well defined electron events later in the day												
1 Aug.	17:29	17:41	17:39	17:56	10	11,340			X	8905	N27	W63	2B
	17:29	17:39	17:42	17:59	13	2,940		X					
	17:29	17:39	17:42	18:01	13	3,500	X						
2 Aug.	17:24	17:31	17:43	18:01	19	430	X			8905	N26	W75	IN
3 Aug.	09:15	09:34	09:43	11:24	28	1,120			X	8905	N27	W86	IN
	09:17	09:35	09:42	10:50	25	430		X					
	09:17	09:35	09:42	10:25	25	360	X						
26 Oct.	06:08	06:17	~ 06:31	~ 07:27	~ 23	11	X			9034	N09	W40	1B
	06:06	06:15	-	-	-	~ 9		X					
29-30 Oct.	23:30	00:04	00:20	01:01	50	140	X			9034	N11	W89	2B
	23:30	-	< 00:24	01:14 (?)	< 54	240		X					
4 Nov.	11:51	12:00	12:11	12:41	20	190	X			9047	S18	W33	1B
	11:51	12:00	12:20	12:57	29	280		X					

J. A. Van Allen and S. M. Krimigis
University of Iowa
29 February 1968

TABLE I

TABLE II

LUNAR EXPLORER 35 COSMIC DUST EXPERIMENT
ACOUSTIC TRANSDUCER SENSOR

DATA: Period from 208/'67 - - 058/'68 (11 days of data gaps)
Time sampled in the 202 days of data = 148.7 days
Events detected = 375
Rate = 2.5 events/day
Projected number of hits for full 202 days = 514

Poisson-predicted distribution if random (2 day intervals):

No. of hits	0 or 1	2	3	4	5	6	7	8	9	or more
Expected distribution of events	4	9	14	18	18	15	11	7	7	
Actual distribution of events	8	14	12	8	15	15	13	5	12	

Chi-squared = 20.46 Probability of randomness: 0.01

TABLE III

LUNAR EXPLORER 35	
Acoustical Transducer: (threshold $\doteq$ 5 pg)	$5 \times 10^{-4} \leq \Phi \leq 1 \times 10^{-3}$ events/m^2sec
Coincidence of Acoustical Transducer and Impact Capacitor: (threshold $\doteq$ 100 pg)	$\Phi \doteq 1.2 \times 10^{-5}$ events/m^2sec
LUNAR ORBITER	
Penetration Sensors: (threshold $\doteq$ 1 ng)	$\Phi \doteq 1.8 \times 10^{-6}$ penetrations/m^2sec
MARINER IV - INTERPLANETARY SPACE	
Acoustical Transducer: (threshold $\doteq$ 5 pg)	$7 \times 10^{-5} \leq \Phi \leq 3.3 \times 10^{-4}$ events/m^2sec

8.0 List of Figures

1. Projection on ecliptic plane of orbits of Lunar Explorer 35 from 1 August to 31 December 1967. A selenocentric coordinate system is employed with X_{SSE} ≡ Moon-Sun line.

2. Measured integral currents of the retarding potential analyzer in the interval -15V to +15V when Explorer 35 is in solar illumination and lunar shadow (22).

3. Series of electron mode spectra obtained as Explorer 35 passes through lunar wake illustrating progressive changes of the interplanetary plasma as it flows past the moon (22).

4. Measurements of total ion current by MIT plasma cup in range $50 \leq E/Q \leq 2850$ ev as Explorer 35 passes through lunar wake (11). A logarithmic amplitude scale is employed.

5. Orbital position of Explorer 35 and interpretations of MIT plasma data obtained on 27 July 1967, presented in fig. 4 (11).

6. Sum (A+B) and difference (A-B) ion currents of MIT split-collector Faraday cup for an orbital pass at maximum distance behind moon (12).

7. NASA-GSFC measurements of interplanetary magnetic field vector for two passes through lunar wake. Data on 31 July 1967 (a) indicate essentially no effect due to moon or lunar wake while 4 August 1967 data (b) clearly illustrate characteristic + - + - + perturbations of field magnitude. δC and δF represent RMS deviations of components and magnitude computed over 81.9 second interval from 16 sample values (20).

8. NASA-GSFC measurements of interplanetary magnetic field vector in lunar wake at maximum Explorer 35 distance behind the moon on 4 December 1967. Simultaneous data from Explorer 33 is shown for comparison.

9. NASA-GSFC measurements of magnetic field vector in geomagnetic tail near full moon on 19 October as Explorer 35 passes through periselene ($\phi_{SSE} = 0^{o} = 360^{o}$) (3).

10. NASA-ARC measurements of typical interplanetary magnetic field magnitude observed during 4 passes through lunar shadow (5).

11. Features observed by NASA-ARC magnetometer when Explorer 35 passes through lunar wake region and the moon is outside the earth's bow shock (5).

12. U. California, Berkeley results from ion chamber for several orbits as function of time from periselene (10).

13. Geometry of magnetic field lines passing near or through the moon in the context of studying shadowing of electron particle fluxes by the moon (26).

14. Observations by U. California, Berkeley GM tubes of solar electron particle flux shadowing by moon when Explorer 35 and moon are in interplanetary space (10). Field line threading parameters D and Δ computed from NASA-GSFC measurements of vector magnetic field (27).

15. Experimental geometry for Stanford University bistatic radar measurements of electromagnetic properties of lunar surface (26).

16. Observations (solid curve) of occultation immersion behind lunar disk of 136 mHZ spacecraft transmitted signal. Theoretical result is shown as dotted curve (26) for a knife edge.

17(a). Reflectivity of lunar surface versus angle of incidence obtained by Stanford U.

(b). Measurement of Brewster angle of lunar surface (26).

18. Histogram of number of impact events observed by acoustical transducer per 8 day period from 27 July 1967 to 28 February 1968 (1).

19. Theoretical perturbed interplanetary magnetic field F, relative to undisturbed value F_o, in symmetry plane at R/R_M = 1.7 and 4.0 for 3 values of β = 0.5, 1.0 and 2.0 (20).

20. Schematic diagram of solar wind flow past moon forming solar plasma umbra with increased field magnitude and decreases in penumbral regions.

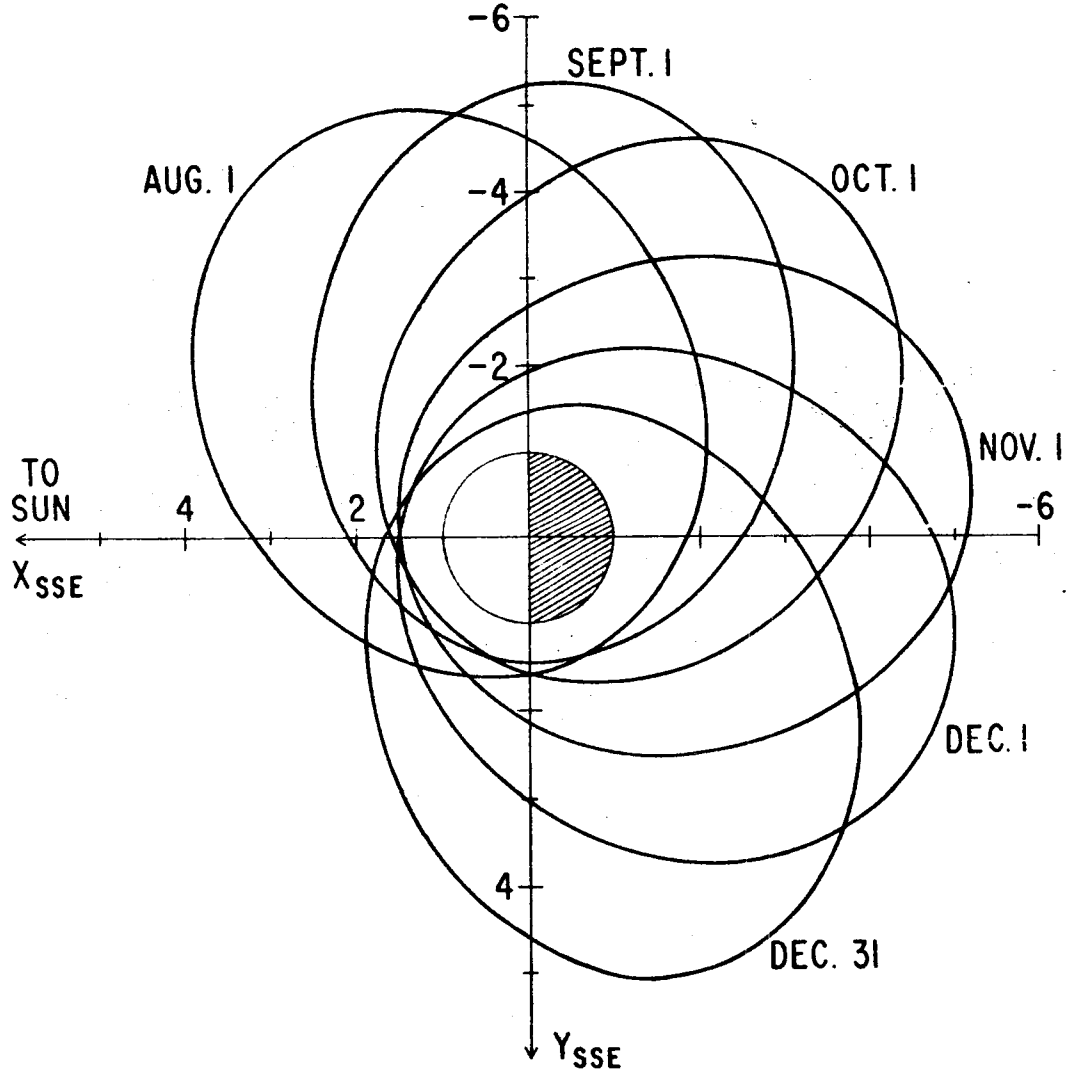

EXPLORER 35 ORBITS, 1967

FIGURE 1

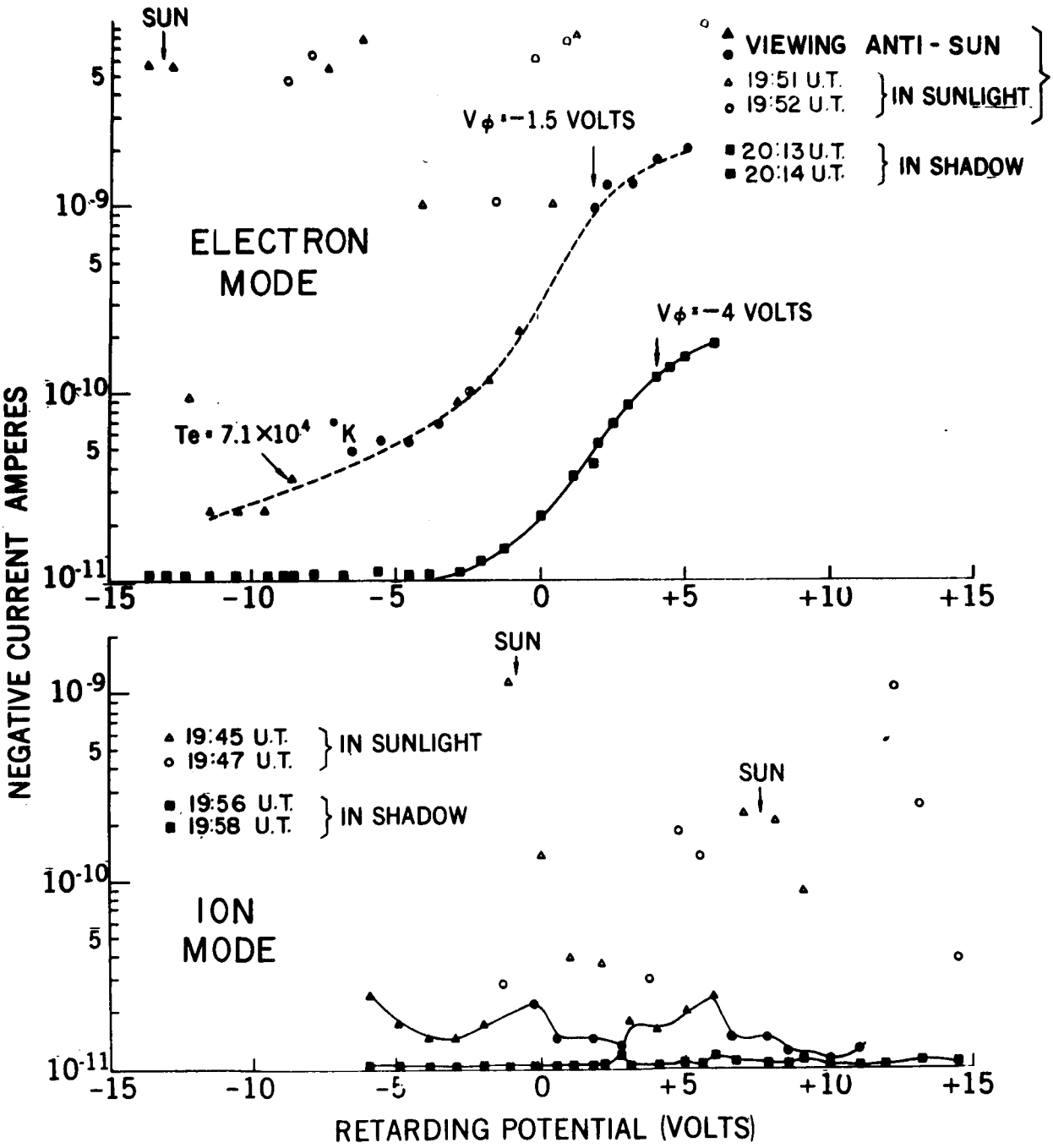
EXPLORER - 35 JANUARY 28, 1968
SUN
VIEWING ANTI - SUN
19:51 U.T.
19:52 U.T.
IN SUNLIGHT
20:13 U.T.
20:14 U.T.
IN SHADOW
Vφ = −1.5 VOLTS
Vφ = −4 VOLTS
ELECTRON MODE
Te = 7.1×10⁴ °K
NEGATIVE CURRENT AMPERES
10⁻⁹
10⁻¹⁰
10⁻¹¹
5
−15
−10
−5
0
+5
+10
+15
SUN
19:45 U.T.
19:47 U.T.
IN SUNLIGHT
19:56 U.T.
19:58 U.T.
IN SHADOW
SUN
ION MODE
RETARDING POTENTIAL (VOLTS)

FIGURE 2

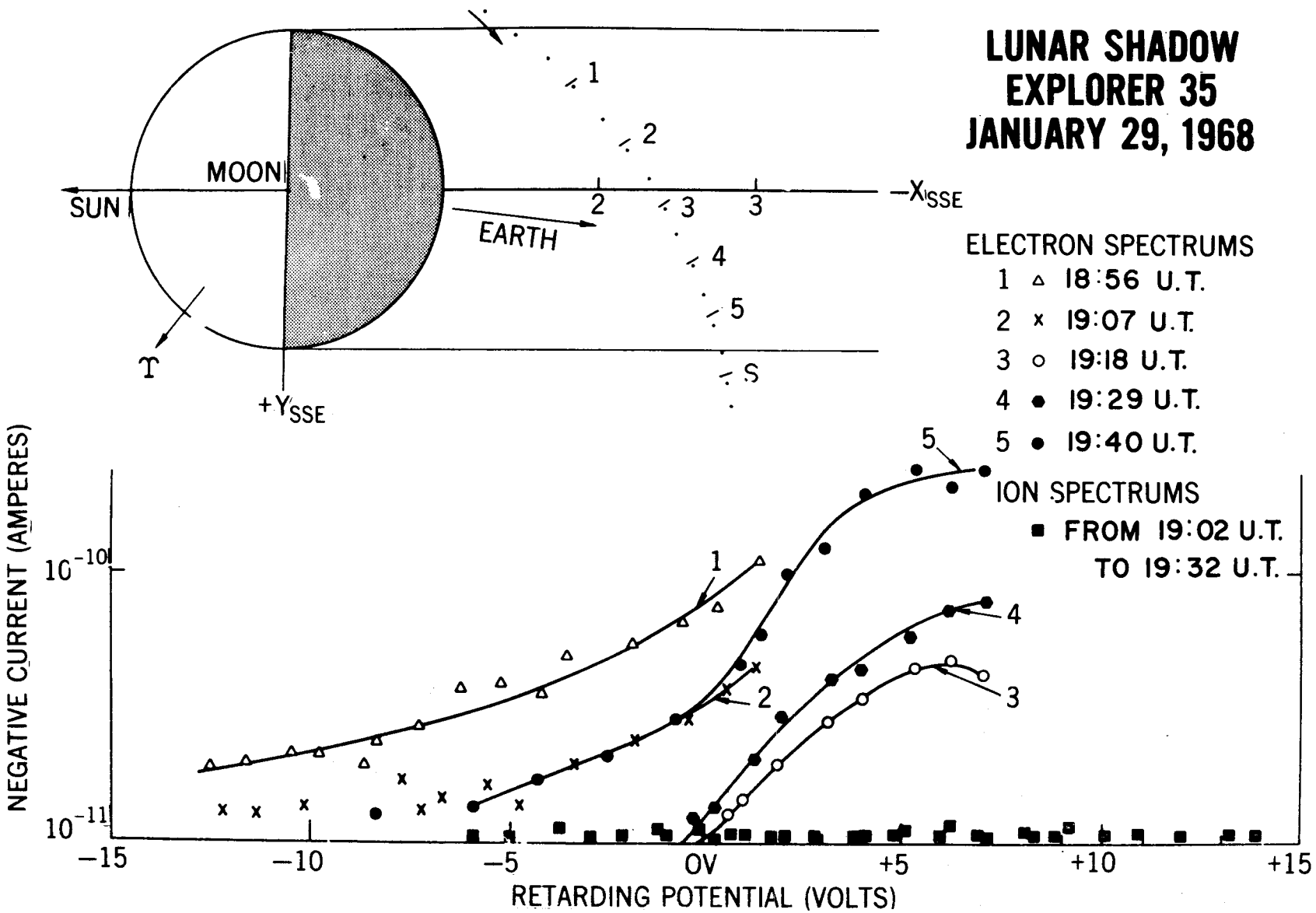
LUNAR SHADOW
EXPLORER 35
JANUARY 29, 1968
MOON
SUN
EARTH
$-X_{SSE}$
$+Y_{SSE}$
ELECTRON SPECTRUMS
1 △ 18:56 U.T.
2 × 19:07 U.T.
3 ○ 19:18 U.T.
4 ● 19:29 U.T.
5 ● 19:40 U.T.
ION SPECTRUMS
■ FROM 19:02 U.T.
TO 19:32 U.T.
NEGATIVE CURRENT (AMPERES)
10^{-10}
10^{-11}
−15
−10
−5
0V
+5
+10
+15
RETARDING POTENTIAL (VOLTS)

FIGURE 3

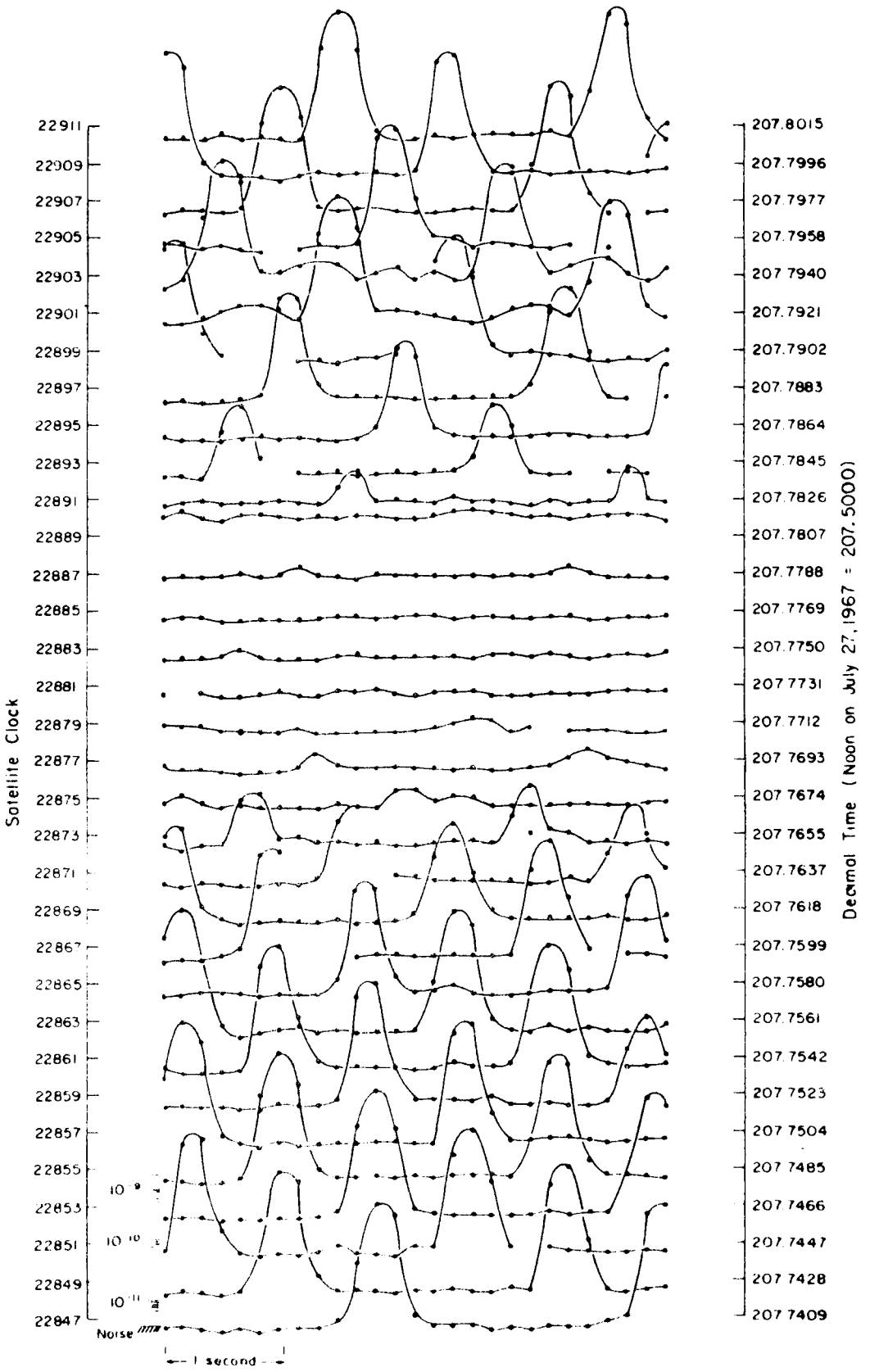
Satellite Clock
22911
22909
22907
22905
22903
22901
22899
22897
22895
22893
22891
22889
22887
22885
22883
22881
22879
22877
22875
22873
22871
22869
22867
22865
22863
22861
22859
22857
22855
22853
22851
22849
22847
Noise
1 second
207.8015
207.7996
207.7977
207.7958
207.7940
207.7921
207.7902
207.7883
207.7864
207.7845
207.7826
207.7807
207.7788
207.7769
207.7750
207.7731
207.7712
207.7693
207.7674
207.7655
207.7637
207.7618
207.7599
207.7580
207.7561
207.7542
207.7523
207.7504
207.7485
207.7466
207.7447
207.7428
207.7409
Decimal Time (Noon on July 27, 1967 = 207.5000)

FIGURE 4

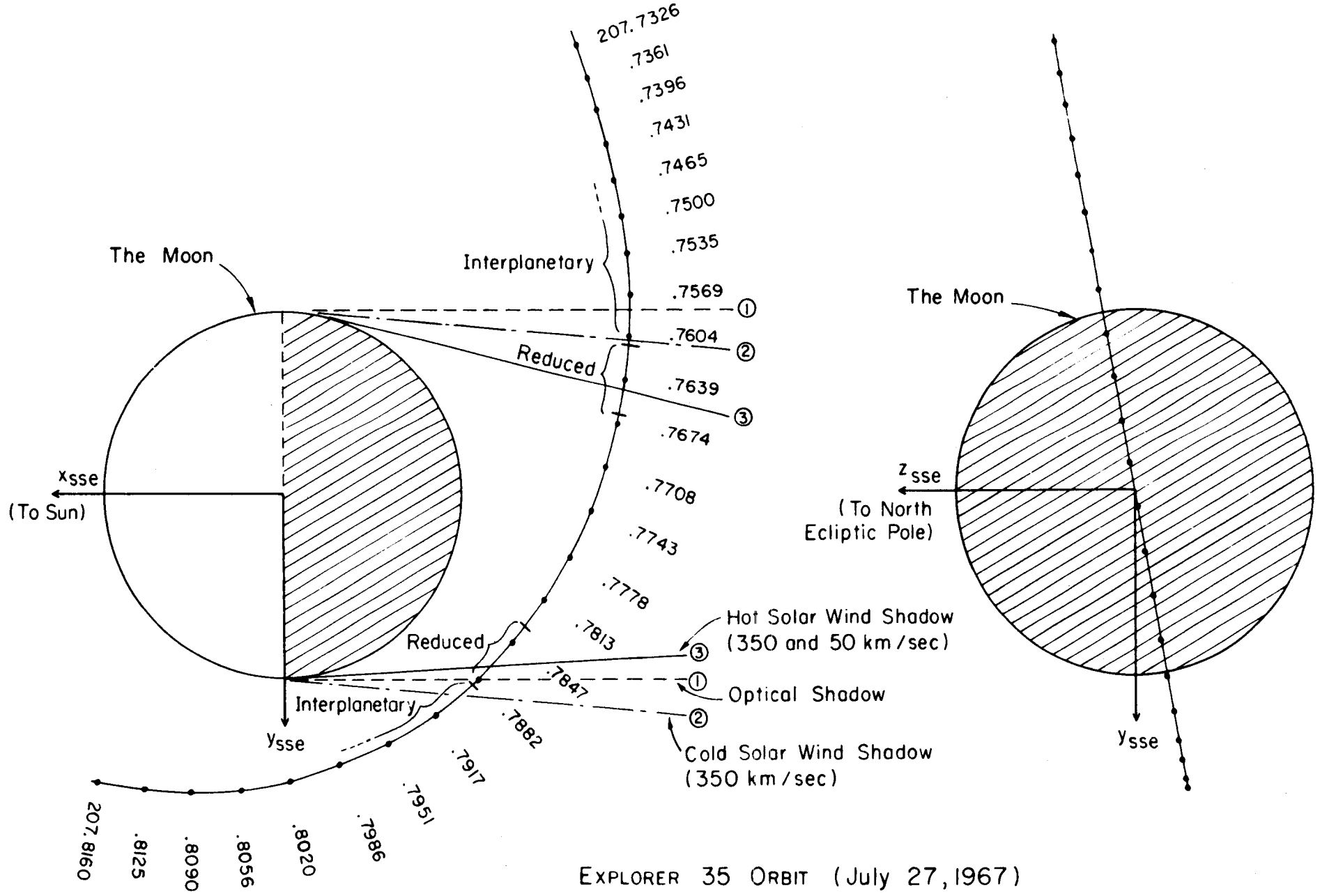

EXPLORER 35 ORBIT (July 27, 1967)

FIGURE 5

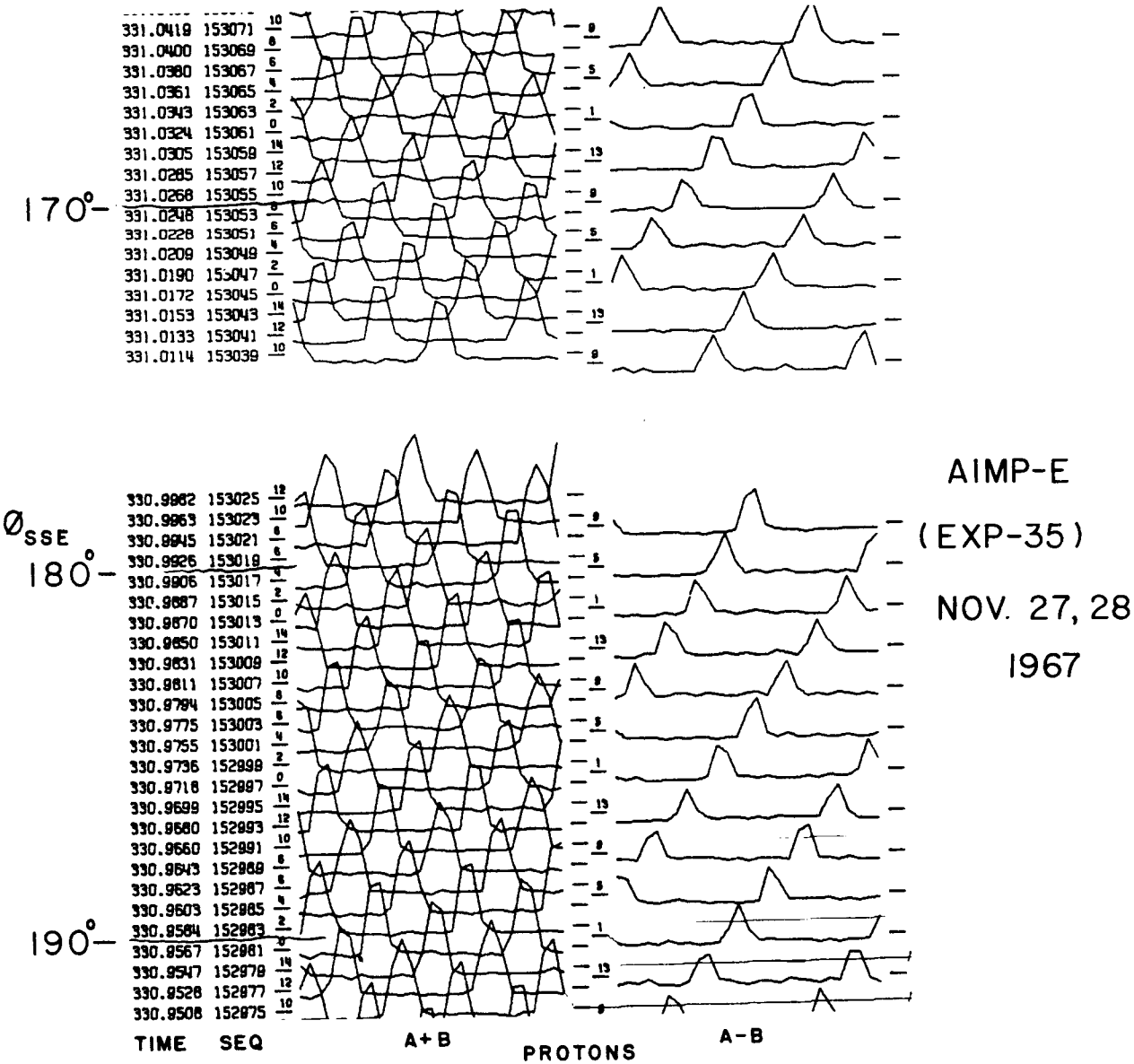
170°
180°
190°
ϕ_{SSE}
331.0419 153071
331.0400 153069
331.0380 153067
331.0361 153065
331.0343 153063
331.0324 153061
331.0305 153058
331.0285 153057
331.0268 153055
331.0248 153053
331.0228 153051
331.0209 153049
331.0190 153047
331.0172 153045
331.0153 153043
331.0133 153041
331.0114 153039
330.9982 153025
330.9963 153023
330.9945 153021
330.9926 153019
330.9906 153017
330.9887 153015
330.9870 153013
330.9850 153011
330.9831 153009
330.9811 153007
330.9794 153005
330.9775 153003
330.9755 153001
330.9736 152998
330.9718 152997
330.9699 152995
330.9680 152993
330.9660 152991
330.9643 152989
330.9623 152987
330.9603 152985
330.9584 152983
330.9567 152981
330.9547 152979
330.9528 152977
330.9508 152975
TIME SEQ
A+B
A-B
PROTONS
AIMP-E
(EXP-35)
NOV. 27, 28
1967

FIGURE 6

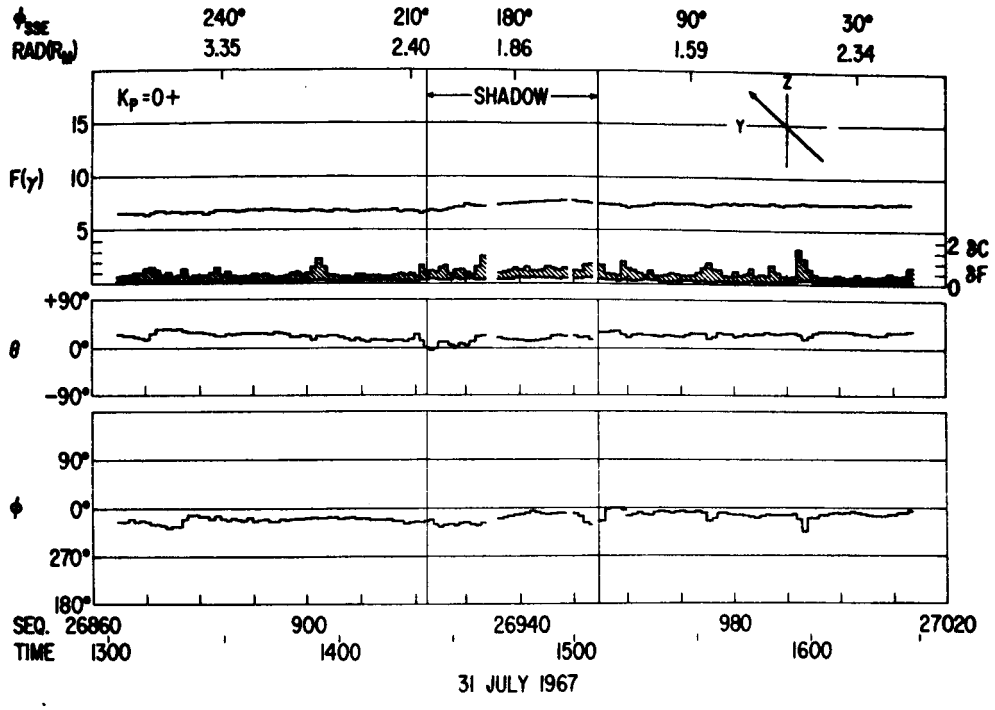
ϕ_{SSE} 240° 210° 180° 90° 30°
RAD(R_M) 3.35 2.40 1.86 1.59 2.34
K_p=0+
SHADOW
Z
Y
15
F(y) 10
5
2 δC
0 δF
+90°
θ 0°
-90°
90°
φ 0°
270°
180°
SEQ. 26860 900 26940 980 27020
TIME 1300 1400 1500 1600
31 JULY 1967

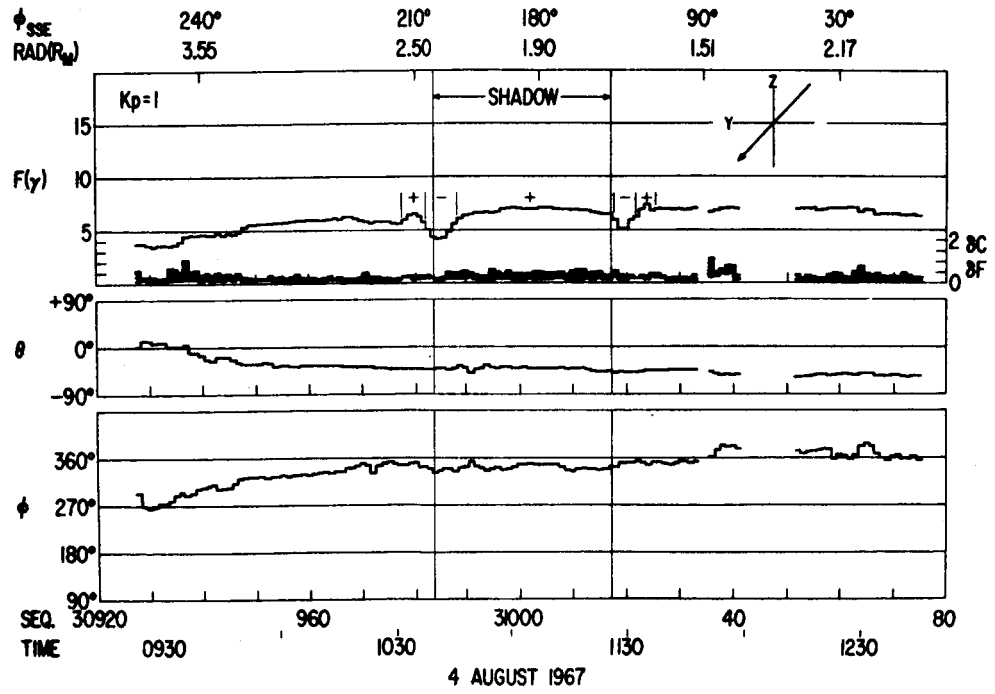
ϕ_{SSE} 240° 210° 180° 90° 30°
RAD(R_M) 3.55 2.50 1.90 1.51 2.17
Kp=1
SHADOW
Z
Y
15
F(y) 10
5
2 δC
0 δF
+90°
θ 0°
-90°
360°
φ 270°
180°
90°
SEQ. 30920 960 31000 40 80
TIME 0930 1030 1130 1230
4 AUGUST 1967

FIGURE 7

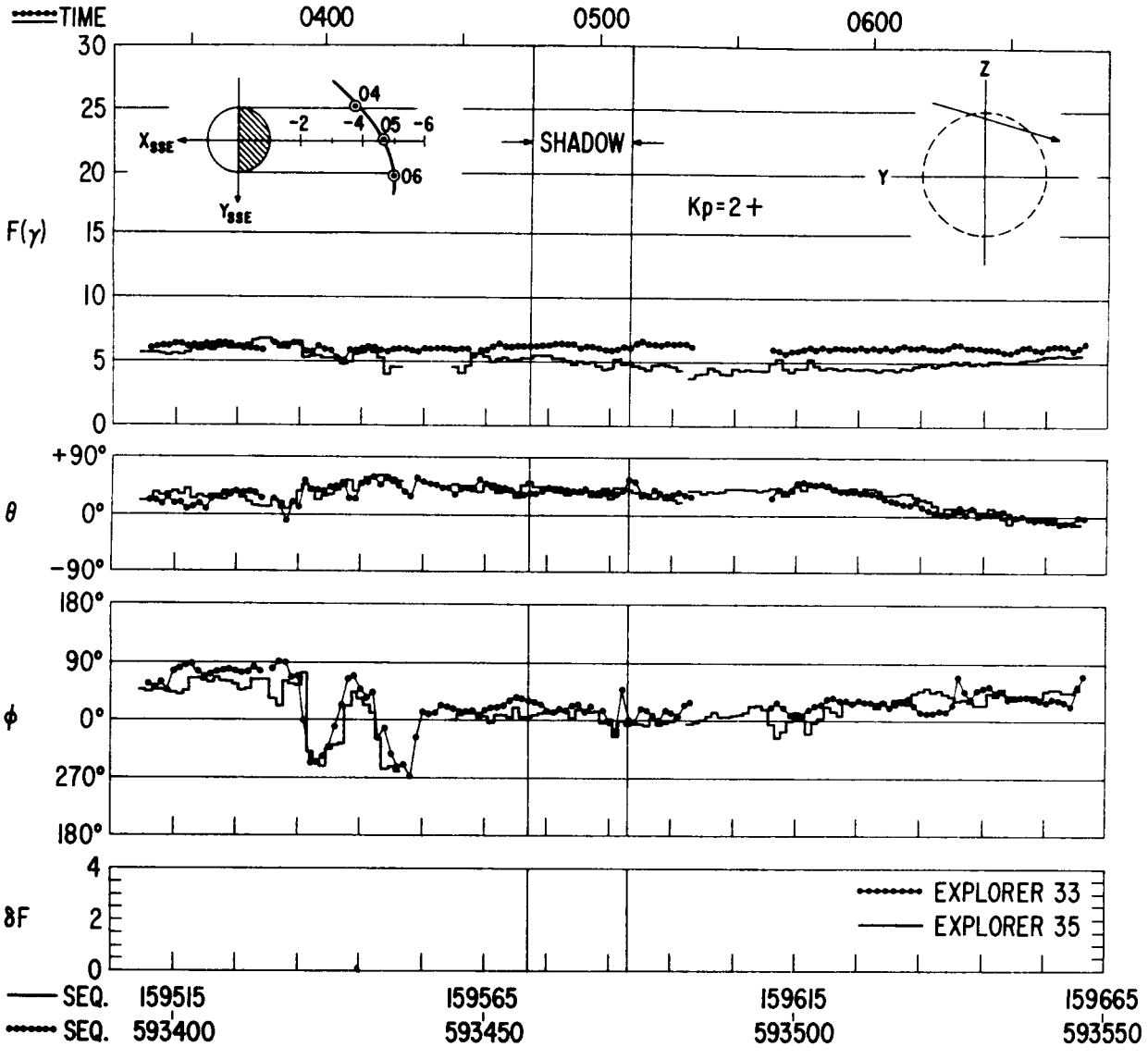

EXPLORERS 33 & 35 - 4 DECEMBER 1967

FIGURE 8

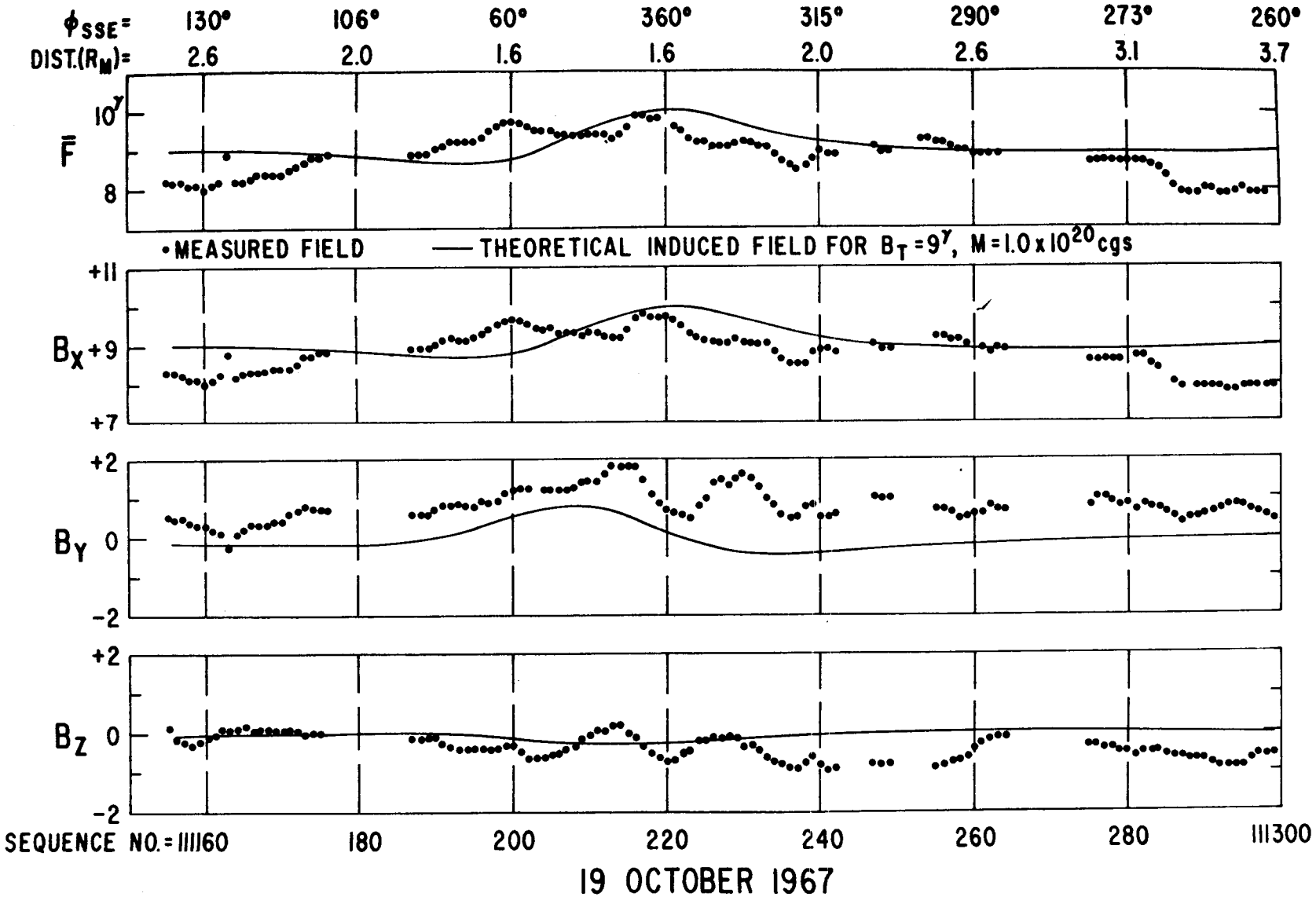
ϕ_{SSE}= 130° 106° 60° 360° 315° 290° 273° 260°
DIST.(R_M)= 2.6 2.0 1.6 1.6 2.0 2.6 3.1 3.7
$\bar{F}$
10γ
8
• MEASURED FIELD — THEORETICAL INDUCED FIELD FOR B_T = 9γ, M = 1.0 x 10^{20} cgs
B_X
+11
+9
+7
B_Y
+2
0
-2
B_Z
+2
0
-2
SEQUENCE NO.= 111160 180 200 220 240 260 280 111300
19 OCTOBER 1967

FIGURE 9

EXPLORER 35, AMES MAGNETOMETER
WEIGHTED AVERAGE MAGNETIC FIELD MAGNITUDE
FOUR PASSES THROUGH LUNAR SHADOW
AUGUST 4-9, 1967

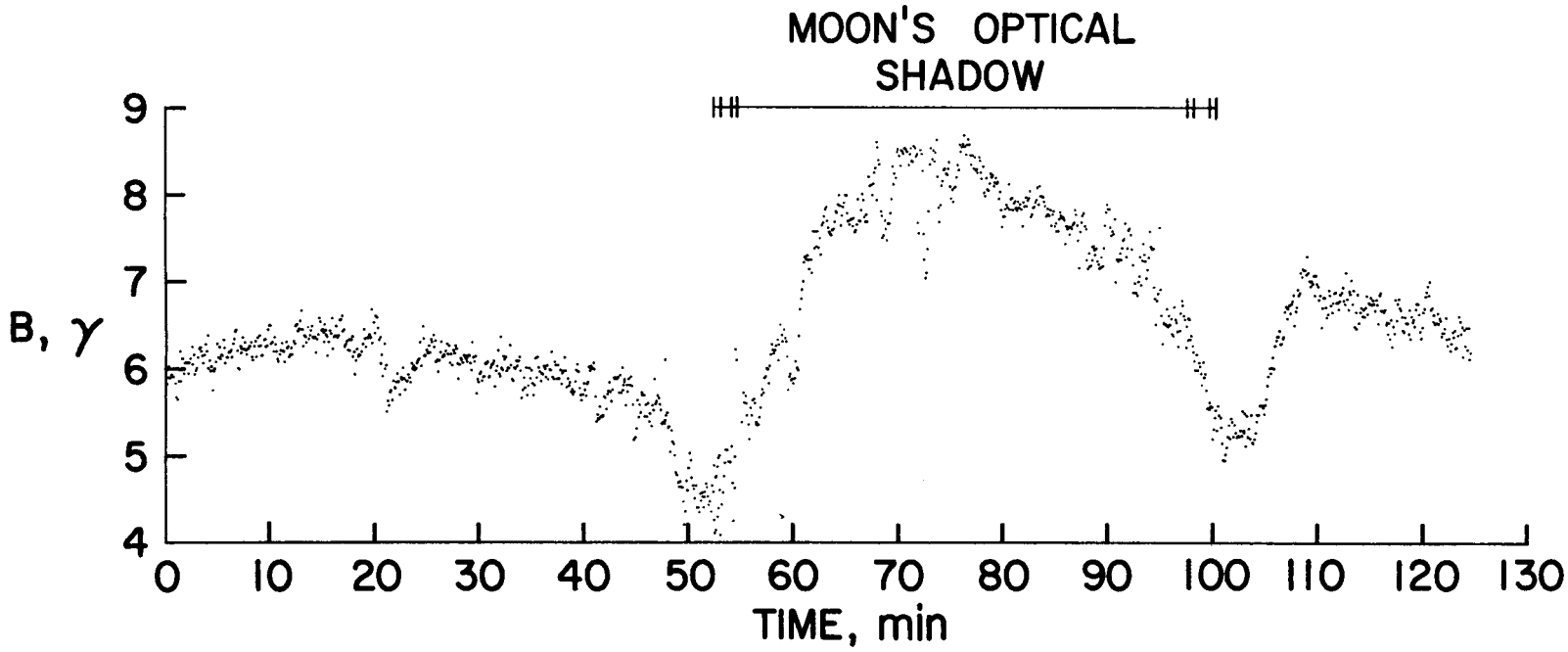

FIGURE 10

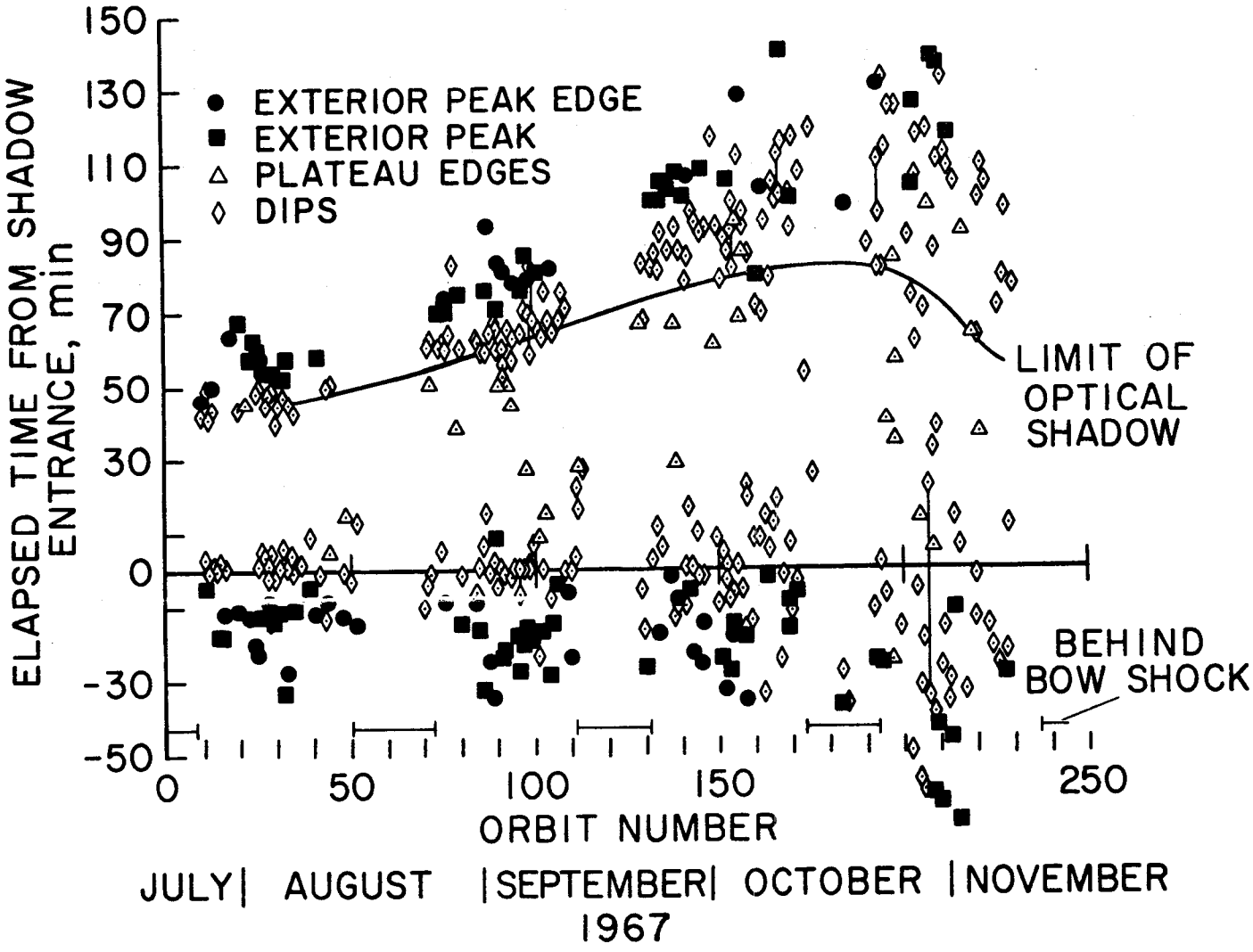
LOCATION OF LUNAR CAVITY FEATURES
EXPLORER 35 AMES MAGNETOMETER EXPERIMENT
ELAPSED TIME FROM SHADOW ENTRANCE, min
150
130
110
90
70
50
30
0
-30
-50
EXTERIOR PEAK EDGE
EXTERIOR PEAK
PLATEAU EDGES
DIPS
LIMIT OF OPTICAL SHADOW
BEHIND BOW SHOCK
0
50
100
150
250
ORBIT NUMBER
JULY
AUGUST
SEPTEMBER
OCTOBER
NOVEMBER
1967

FIGURE 11

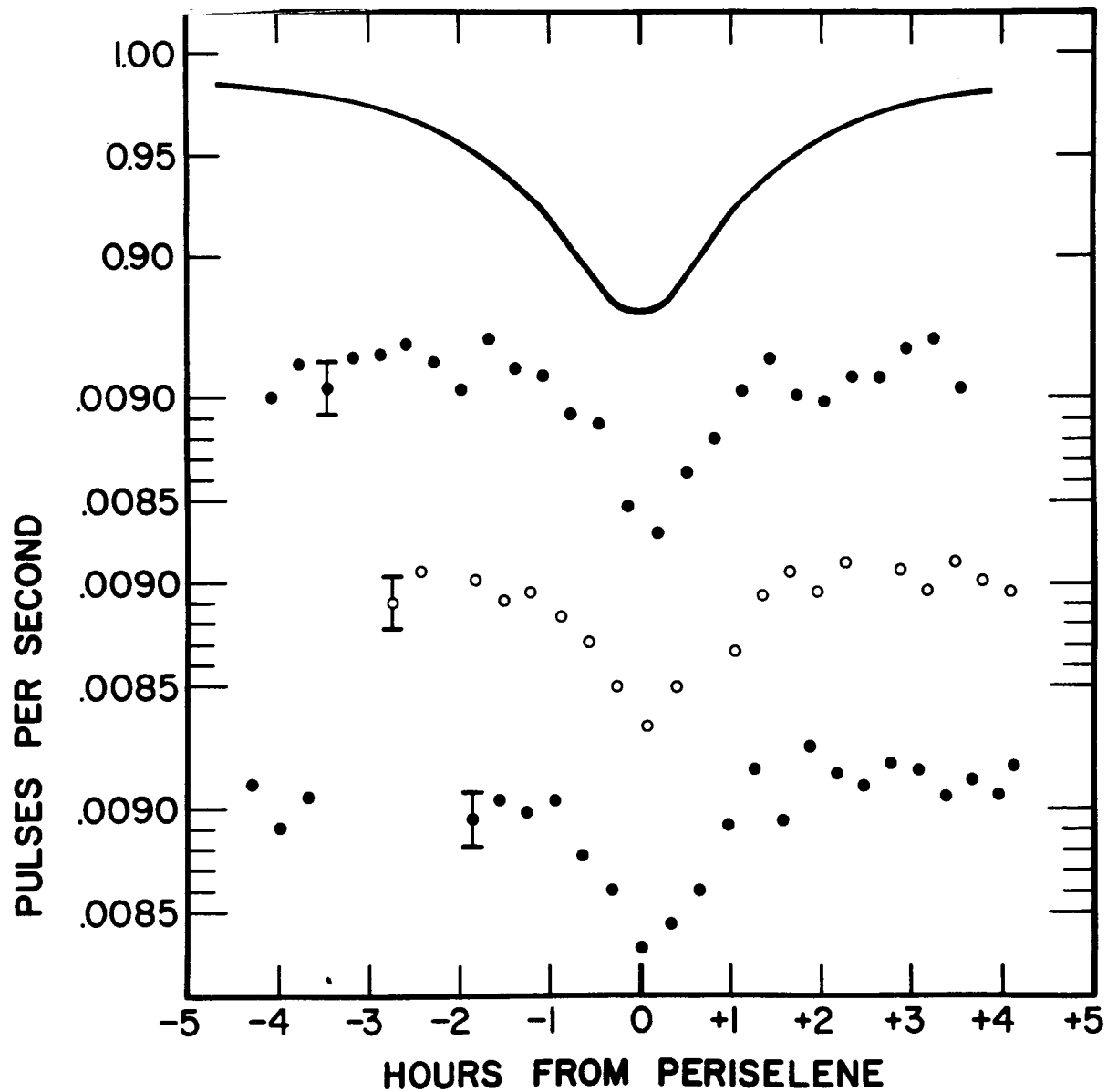
1.00
0.95
0.90
.0090
.0085
.0090
.0085
.0090
.0085
PULSES PER SECOND
-5
-4
-3
-2
-1
0
+1
+2
+3
+4
+5
HOURS FROM PERISELENE

FIGURE 12

FIELD LINE THREADING OF MOON

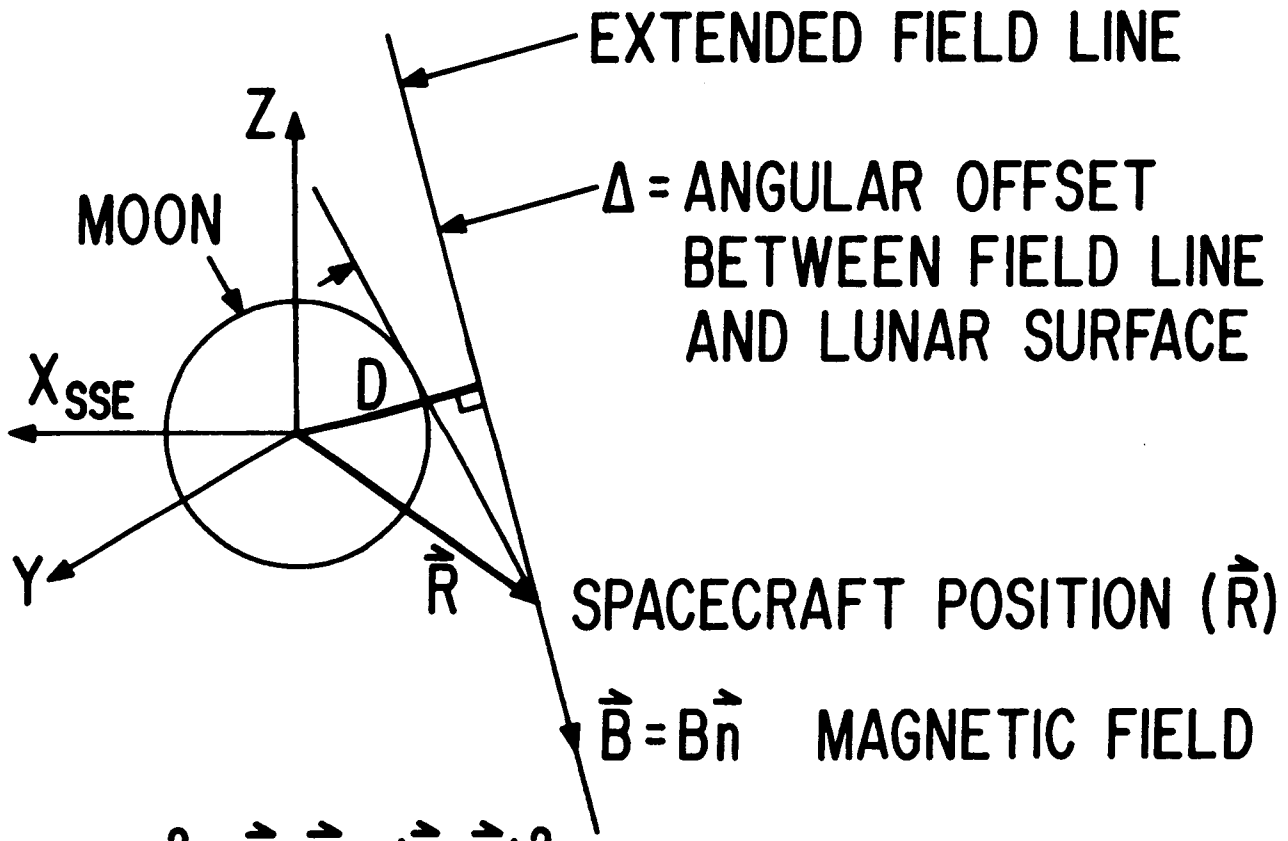

$$D^2 = \vec{R}\cdot\vec{R} - (\vec{R}\cdot\vec{n})^2$$

$$\Delta = \tan^{-1}\left(D/|\vec{R}\cdot\vec{n}|\right) - \tan^{-1}\left(1/\sqrt{R^2-1}\right)$$

FIGURE 13

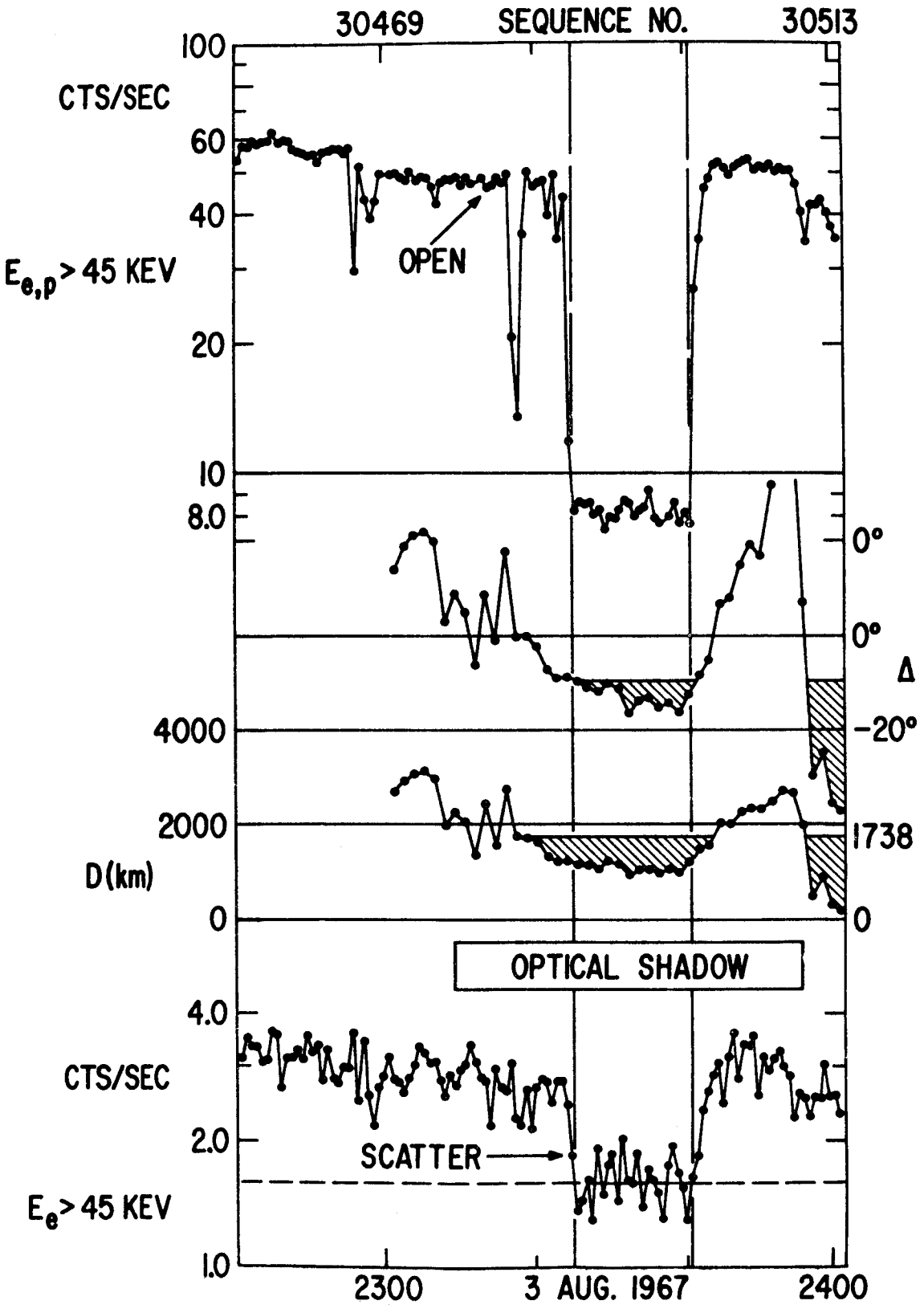
30469
SEQUENCE NO.
30513
100
CTS/SEC
60
40
$E_{e,p}$ > 45 KEV
OPEN
20
10
8.0
0°
0°
Δ
-20°
4000
2000
1738
D(km)
0
0
OPTICAL SHADOW
4.0
CTS/SEC
2.0
SCATTER
E_e > 45 KEV
1.0
2300
3 AUG. 1967
2400

FIGURE 14

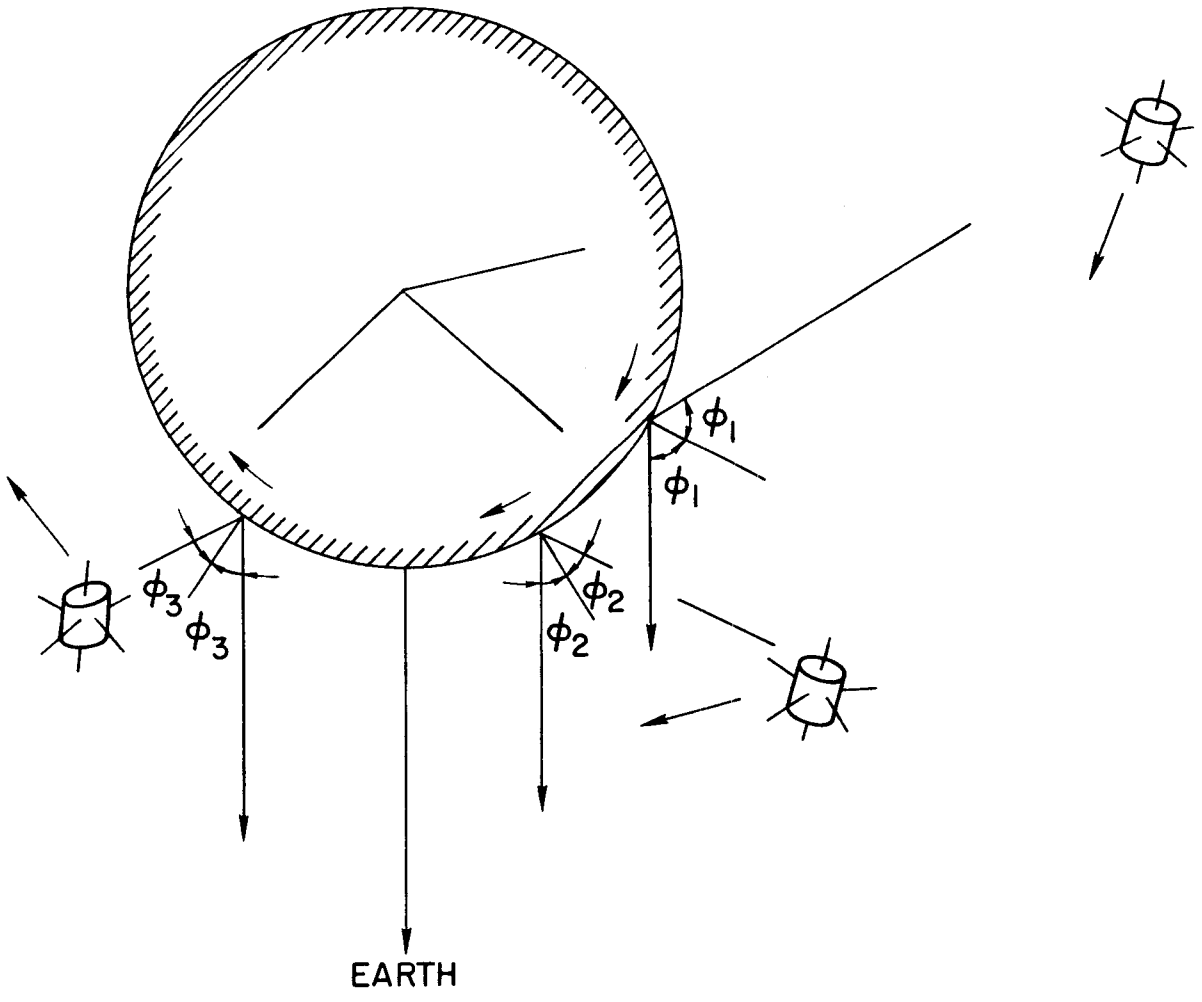

FIGURE 15

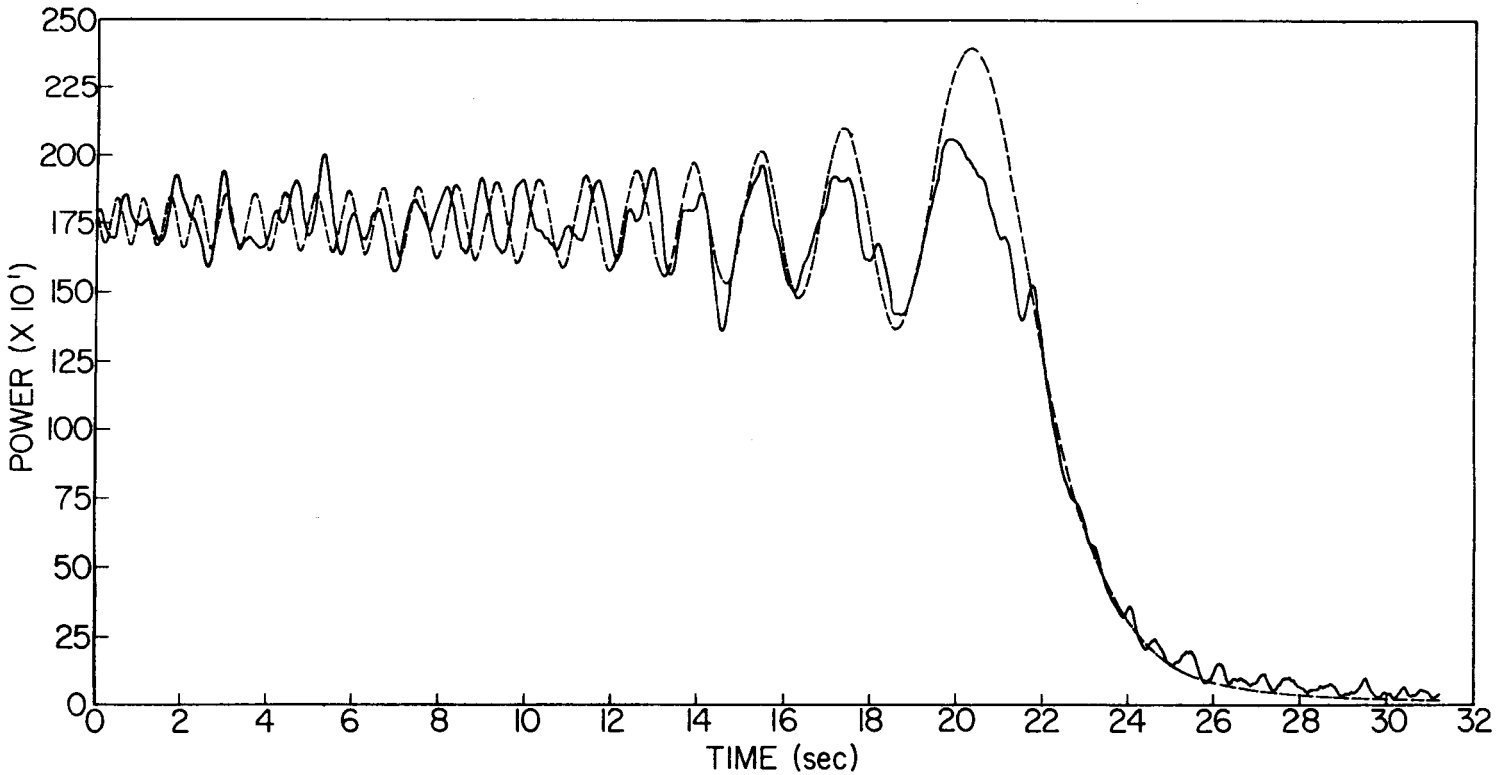
250
225
200
175
150
125
100
75
50
25
0
POWER (X 10')
0
2
4
6
8
10
12
14
16
18
20
22
24
26
28
30
32
TIME (sec)

FIGURE 16

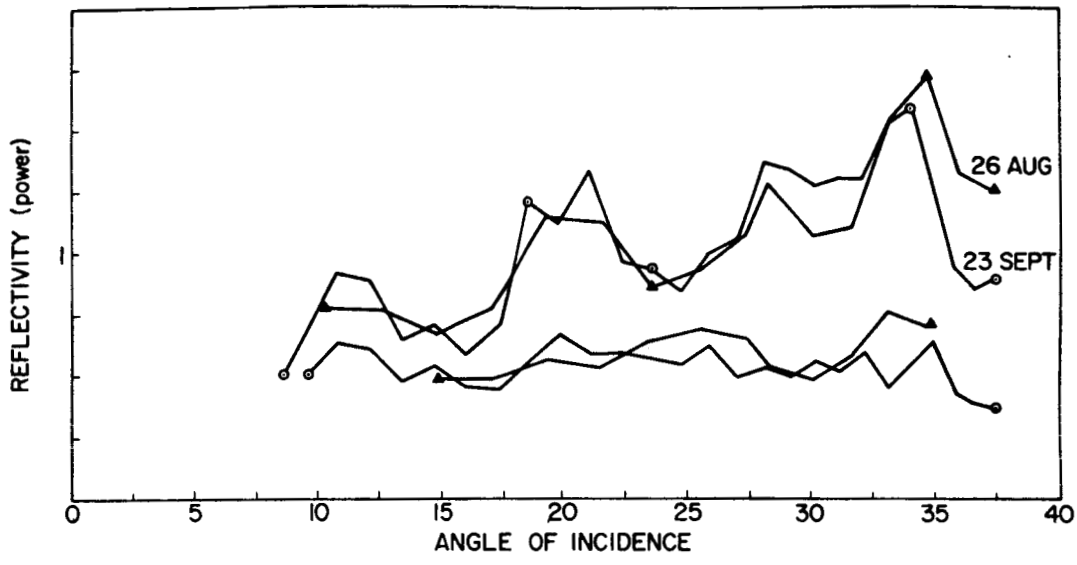
REFLECTIVITY (power)
26 AUG
23 SEPT
0
5
10
15
20
25
30
35
40
ANGLE OF INCIDENCE

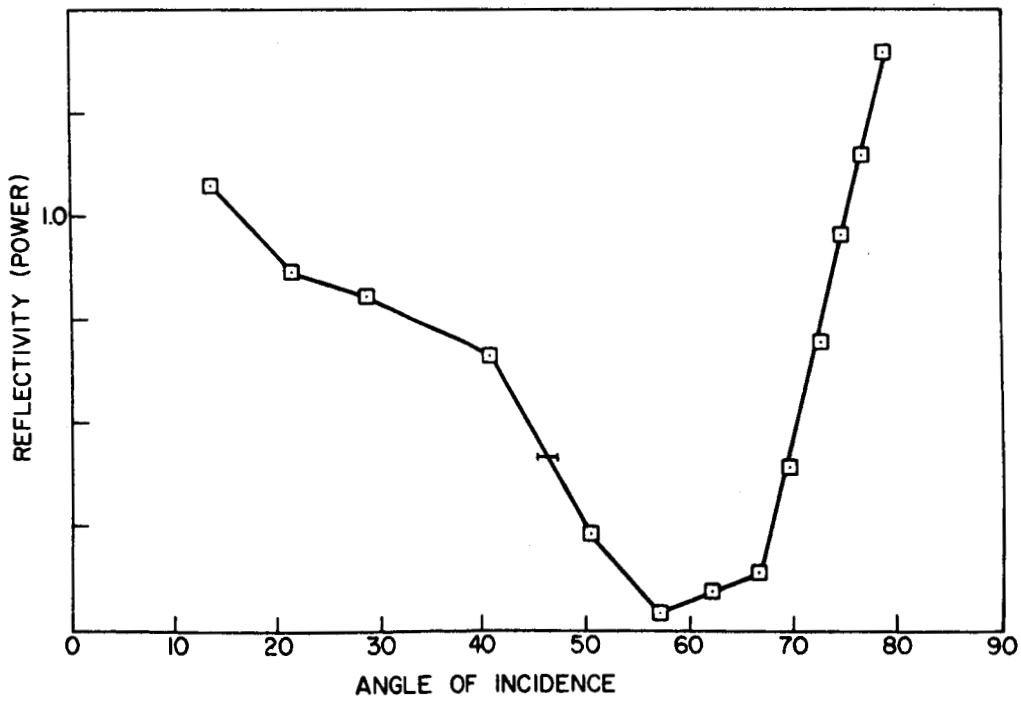
REFLECTIVITY (POWER)
1.0
0
10
20
30
40
50
60
70
80
90
ANGLE OF INCIDENCE

FIGURE 17

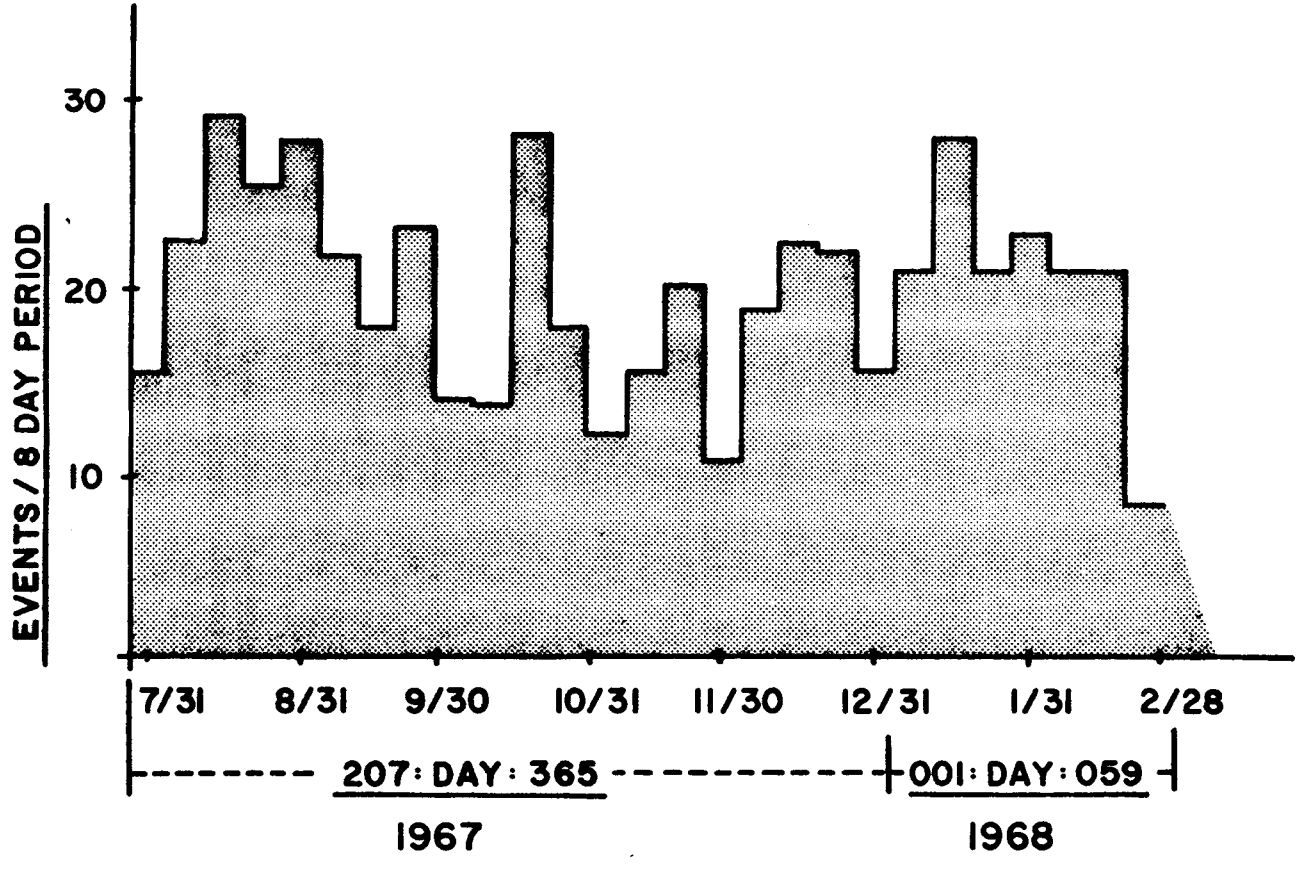
EVENTS / 8 DAY PERIOD
30
20
10
7/31
8/31
9/30
10/31
11/30
12/31
1/31
2/28
207: DAY: 365
001: DAY: 059
1967
1968

FIGURE 18

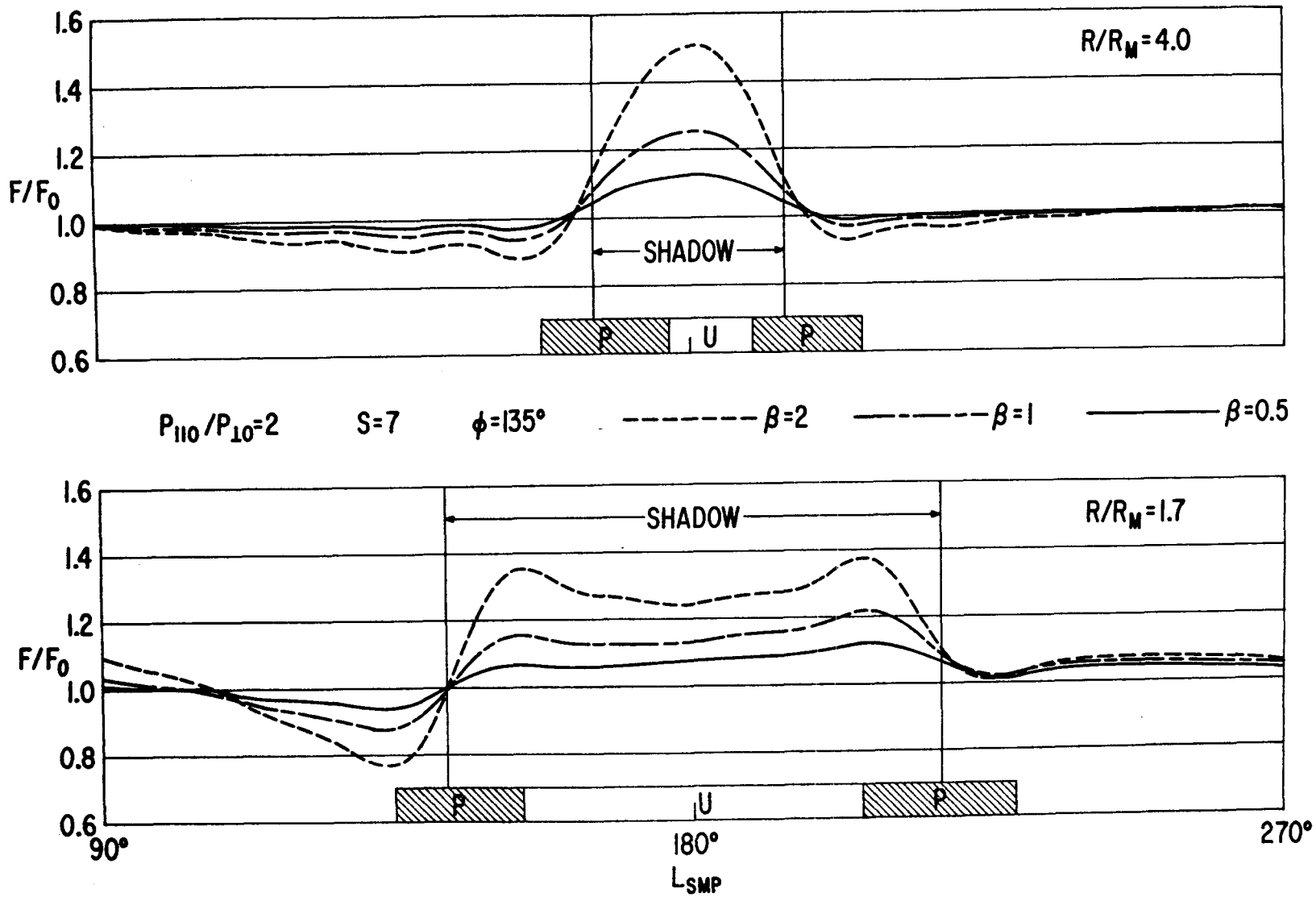
1.6
1.4
1.2
F/F0
1.0
0.8
0.6
R/RM=4.0
SHADOW
P
U
P
P110/P⊥0=2
S=7
φ=135°
β=2
β=1
β=0.5
1.6
1.4
1.2
F/F0
1.0
0.8
0.6
SHADOW
R/RM=1.7
P
U
P
90°
180°
270°
LSMP

FIGURE 19

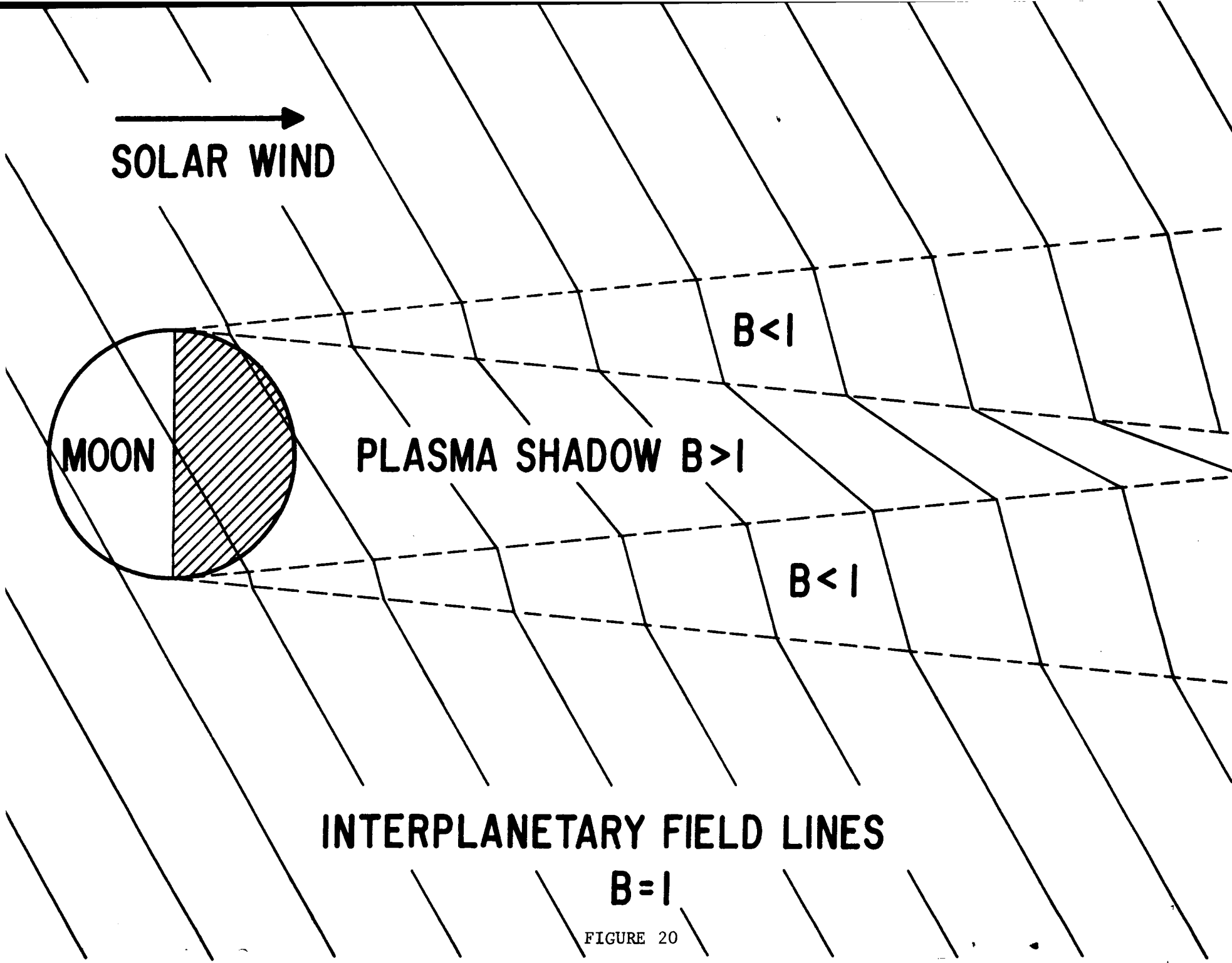
SOLAR WIND
B<1
MOON
PLASMA SHADOW B>1
B<1
INTERPLANETARY FIELD LINES
B=1

FIGURE 20